Receptor modulated assembly and drug induced disassembly of amyloid beta aggregates at asymmetric neuronal model biomembranes

Nirod Kumar Sarangi,[1, 2] Subrata Mondal[1, 2] and Tia E Keyes[1]*

[1]School of Chemical Sciences, Dublin City University, Dublin 9, Ireland

[2] Insight Centre For Data Analytics, Dublin City University, Dublin 09, Ireland

Corresponding author, Email: tia.keyes@dcu.ie

Abstract:

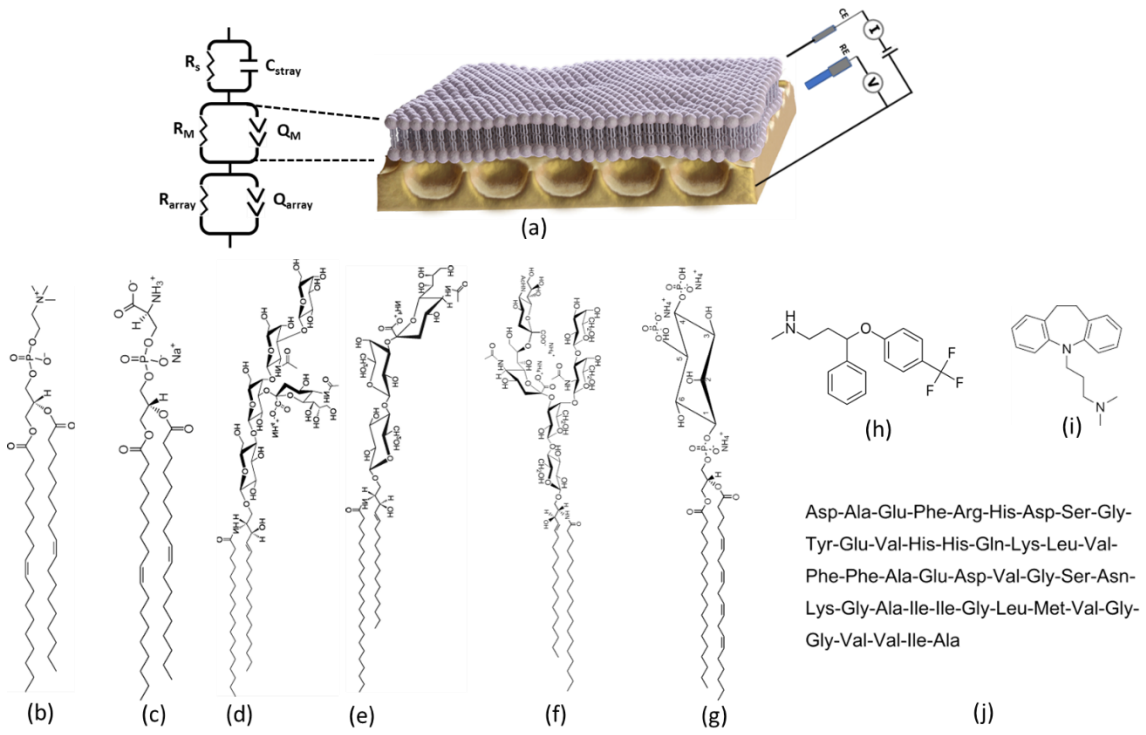
Amyloid peptide non-fibrillar oligomers cause neurotoxicity and may contribute to Alzheimer's disease (AD) pathogenesis. Mounting evidence indicates that $A\beta_{1-42}$ oligomers disrupt and remodel neuronal membrane, causing neuronal cell death. The involvement of individual neuronal membrane constituents in real-time $A\beta_{1-42}$ aggregate assembly is unclear due to complexity of neuronal cell membrane. We used non-Faradaic electrochemical impedance spectroscopy (EIS) to track monomeric $A\beta_{1-42}$ peptide binding and aggregation pathways in real-time in asymmetric micropore suspended lipid bilayer membranes with anionic phospholipids and glycosphingolipids. Anionic DOPC:PIP2 pore suspended membrane showed pore-formation within 2 hours of incubation, but peptide insertion occurred over 6 hours, with an onset time of ~6-8 hours for peptide aggregation at the membrane surface. Among different gangliosides, peptide binding to GM1- and GM3-containing membranes did not result pore development, but receptor mediated peptide aggregation formation caused membrane admittance to decrease within 2 hours. In contrast, partial peptide insertion in the membrane surface increases membrane admittance at GD1a and mixed GSL membranes, arresting aggregation. Time-lapsed AFM imaging at asymmetric solid supported lipid bilayers (aSLBs) corroborated EIS findings, capturing pore-formation and receptor mediated peptide assembly routes. Fluorescence lifetime imaging (FLIM) imaging and spatial resolved single-point fluorescence correlation spectroscopy (FCS) at aSLBs revealed membrane-peptide interaction, assembly, and peptide induced membrane reorganisation. Treatment with antidepressants fluoxetine and imipramine therapeutics in synergy which are cost-effective and capable of crossing, resulted in the disassembly of membrane mediated $A\beta_{1-42}$ aggregates, but not fibrils. Overall, the data suggests that membrane-mediated aggregate disassembly at the correct timing of AD progression may halt or reverse amyloid assembly through the use of repurposed drugs.

Keywords: Pore suspended lipid bilayer; amyloid-beta; drug synergism action; peptide-membrane interaction; lipid and peptide diffusion; fluorescence correlation spectroscopy; electrochemical impedance spectroscopy

1. Introduction

Alzheimer's Disease (AD) is a progressive neurodegenerative disease, diagnosed by cognitive dysfunction and behavioural changes.[1] The amyloid plaques originating from the self-assembly of amyloid β (Aβ) peptides enriched in β sheet conformers, are the common hallmarks of this disease. Thus, inhibiting Aβ aggregation is one of the promising therapeutic approaches proposed to slow the progression of the disease. Multiple lines of evidence shows that few anti-depressants have the potential to regulate amyloid metabolism and toxicity.[2] Imipramine and fluoxetine, both prevalent antidepressants classified as selective serotonin reuptake inhibitors (SSRIs) are known to reduce overall Aβ levels in brain interstitial fluid (ISF) by 25%. Aβ-induced toxicity was shown to be greatly reduced by fluoxetine at therapeutic concentrations (100 nM-10 μM) in mixed glia-neuronal cultures.[3] In humans, cumulative antidepressant use within the 5-year period preceding positron emission tomography (PET) imaging correlated with less plaque load in patients suggesting antidepressant drug as safe alternatives for AD inhibition. However, there is significant cross-talk regarding the impact of antidepressants on AD. While many studies, as outlined above, show impact some studies have shown no effect.[4–7] So far, it appears that these drugs reduce the likelihood of acquiring the disease without slowing its progression.[8,9] Thus, further research is needed into the molecular background behind the impact of SSRIs on AD. However, understanding pharmacological effect in AD at the molecular level in live cells is challenging given the complexity of the neuronal membrane which is crowded, asymmetric and highly dynamic.[10] Thus, model neuronal membrane can both provide new insights into the extent to which neuronal membrane receptors drive Aβ binding and assembly from its monomeric counterpart, and aid in identifying drug candidates that are capable disassembling such membrane mediated Aβ aggregates.

Recent studies suggest that two peptides, $A\beta_{1-40}$ and $A\beta_{1-42}$ plays crucial role in amyloid toxicity and contribute maximum to the disease.[11] While Aβ monomers are known to have physiological roles, many lines of evidence indicate Aβ aggregates are neurotoxic and kills neuronal cells.[12] The individual amyloid peptides (especially $A\beta_{1-42}$) spontaneously self-assemble into larger structures such as oligomers, protofibrils, fibrils, and at elevated concentration in membrane free environment.[13] However, at physiological concentrations (nano to sub micromolar concentrations), $A\beta_{1-42}$ assembly is triggered when it meets the lipid bilayer interface.



Scheme 1. Schematic representation of microcavity suspended lipid bilayer (MSLB) over gold used in this work for electrochemical impedance spectroscopy (EIS) along with equivalent circuit model (ECM) to fit EIS data. In ECM, a parallel circuit of R_M and Q_M represents lipid bilayer membrane resistance and constant phase element (CPE) respectively and is connected in series with parallel circuit R_{array} (buffer filled cavity array resistance) and Q_{array} (buffer filled cavity array CPE) and parallel circuit of R_s (solution resistance) and C_{stray} (stray capacitance). Chemical structure of (b) DOPC, (c) DOPS, (d) GM1, (e) GM3, (f) GD1a, (g) PIP2, (h) fluoxetine, (i) imipramine and (j) $A\beta_{1\text{-}42}$.

From the viewpoint of neuronal membrane receptors, gangliosides are important constituent of the central nervous system and have been shown to act as receptor sites for Aβ binding and fibril assembly. Gangliosides, including GM1, constitute 1–2% of the extracellular leaflet of the neuronal plasma membranes [14] where they are particularly highly concentrated within sphingomyelin- and cholesterol-rich lipid rafts via their ceramide tails.[15,16] Ganglioside-enriched microdomains in neuronal membranes are implicated in the onset of Alzheimer's disease.[17,18] Yanagisawa et al.[19] originally described ganglioside-bound Aβ complex as an endogenous seed for Aβ assembly at neuronal membranes and this was later shown at ganglioside-containing model liposomal membranes.[20,21] Sato et al. observed spherical assembly of Aβ-protein at GM1 domains but not at other ganglioside clusters using atomic force microscopy in supported lipid bilayer composed of lipids extracted from detergent-resistant membrane microdomain (DRM) fraction of synaptosomes prepared from aged mouse brain.[22] The size and shape of Aβ fibrils induced by ganglioside nanoclusters were significantly influenced by membrane composition, incubation time, ganglioside's content, the

positional rearrangement of sialyl oligosaccharides (terminal versus branched), galactose, and as well as the number of N-acetylneuraminic acid (NA).[23] Cell-based studies in animal and human models have revealed toxicity of the ganglioside-Aβ complex.[24,25] Additional receptors, including phosphatidylserine and phosphatidylinositol, are primarily located in the cytoplasmic leaflet of the neuronal membrane. However, under situations such as oxidative stress, these lipids are translocated to the exofacial location, signalling cellular apoptosis—a hallmark of Alzheimer's disease. We recently established that the binding of monomeric $A\beta_{1-42}$ to anionic phosphatidylserine (DOPS) results in the development of multilayer and globular peptide aggregates.[26] Aβ concentration typically exists in the picomolar range under physiological conditions.[27] $A\beta_{1-42}$ in its oligomeric form has been demonstrated to interact with model membranes by various mechanisms, including carpet-like oligomer growth assembly, toroidal pore development, and detergent-like effects that result in the extraction of lipid patches from the bilayer surface.[28]Thus, unravelling the involvement of different neuronal membrane receptors in amyloid peptide assembly and peptide-induced membrane heterogeneity[29–31] may support the discovery of new or repurposed AD therapeutics.

In last few decades, several therapeutic strategies targeting Alzheimer's Disease (AD) have been developed. However, most of them have failed in different phases of clinical trials because of inadequate efficacies against AD. For example, in 2021, the US food and drug administration (FDA) green lit Aducanumab, a controversial anti-amyloid immunotherapeutic developed by Biogen and Eisai that was discontinued in 2024.[32] Nonetheless, several anti-amyloid therapies, including gantenerumab, lecanemab, and donanemab, are nearing completion of clinical trials and some therapeutics have already been commercialised. In January 2023, FDA fast-track approval for Lecanemab, after findings from clinical trial that the drug reduced markers of amyloid in early AD and slowed clinical decline in measures of cognition and function by about 27% after 18 months compared to placebo. Treatment by either of these drugs comes with a relatively high annual cost. An attractive alternative to the traditional drug discovery route is the repurposing of existing medications as therapeutics for AD, Repurposing can significantly reduce treatment cost for this disease and speeds up progression to clinical application because repurposed drugs already have established toxicity and safety profiles.[33]To this end, Potter et al.[34] evaluated 595 FDA-approved medicines as apolipoprotein E (APOE) ε4 inhibitors, the latter is responsible for polymerization of Aβ. Of these, they identified imipramine and olanzapine as treatment for Alzheimer's psychiatric symptoms in a neuron cell model, as these drugs can permeate blood-brain-barrier (BBB). Previously, using small molecule-based inhibitors and atomic force microscopy (AFM) imaging, Bieschke et al. have shown that EGCG (polyphenol (-)-epi-gallocatechine gallate) remodels pre-formed $A\beta_{1-42}$ fibrils in a cell-free environment.[35] Another small molecule, curcumin is reported to reduce amyloid beta oligomer interactions with anionic membranes[36], and it

also reduces aggregation of amyloid-beta and disintegrates pre-formed amyloid fibrils and plaques.[37,38]

In this work, we investigate the role of anionic phospholipids and glycosphingolipids on amyloid aggregation and toxicity. Herein, we used pore-suspended and solid-supported asymmetric neuronal model membranes to assess amyloid-lipid interactions in a cell-free biomimetic environment. The model offers a multimodal analytical approach for deep molecular insights into assembly and dynamics of $A\beta_{1-42}$ at membrane interface. We have intensively used Electrochemical impedance spectroscopy and single molecule techniques to monitor peptide aggregation, membrane proration and modulation in membrane admittance properties. Single-point fluorescence correlation spectroscopy (FCS) was used to assess the two-dimensional translational mobility of both lipid and peptide at different time point of lipid-peptide binding. The extent of disassembly of membrane mediated $A\beta_{1-42}$ aggregates using a synergistic effects of repurposed central nervous system permeable (CNS+) antidepressant drugs was monitored using both AFM and FLIM as a mean of for the treatment of early stage of AD pathogenesis using repurposed drugs. The advantage of all of these methods is that they are highly sensitive and suited to working at physiological drug/ amyloid concentrations.

2. Materials and methods

Materials: Lipids such as 1,2-dioleoyl-*sn*-glycero-3-phosphocholine (DOPC), 1,2-dioleoyl-*sn*-glycero-3-phospho-L-serine (DOPS), 1,2-dioleoyl-*sn*-glycero-3-phospho-(1'-myo-inositol-4',5'-bisphosphate) (PI(4,5)P2, ammonium salt) (PIP2), ganglioside GM1 ((brain, ovine-sodium Salt), ganglioside GM3 (milk, bovine-ammonium salt), disialoganglioside-GD1a (porcine brain, diammonium salt), total ganglioside extract (brain, porcine-ammonium Salt), were purchased with maximum degree of purity from Avanti Polar Lipids (Alabama, USA) and used without further purification. 1,2-dioleoyl-*sn*-glycero-3-phosphoethamine labelled Atto532 (ATTO532-PE) and Atto655 (ATTO655-PE) was purchased from ATTO-TEC GmbH (Siegen, Germany). BODIPY™ FL C5-Ganglioside was purchased from Thermo Fisher (Ireland). HEPES salt and sodium azide were purchased from Sigma-Aldrich (Wicklow, Ireland). Human β-Amyloid peptide (1-42) was purchased from Biolegend UK Ltd (London, UK) and Beta-Amyloid (1-42), HiLyte™ Fluor 555-labeled was obtained from Eurogentec (Seraing, Belgium). Gold on silicon wafers were purchased from Ams Biotechnology (Abingdon, UK). Polybead microspheres of different sizes were purchased from Polysciences Europe Gmbh (Baden-Württemberg, Germany). Aqueous solutions were prepared using MilliQ water (18mΩ cm) (Milipore Corp. Bedford, USA). Polydimethylsiloxane silicon elastomer (PDMS) was purchased from Dow Corning Gmbh (Wiesbaden, Germany) and mixed following supplier's instructions. 1,1,1,3,3,3-hexafluoroisopropanol (HFIP).

2.1 Vesicle preparation: Different large unilamellar vesicles (LUVs) such as DOPC, DOPC:DOPS (90:10), DOPC:GM1 (99:1), DOPC:GM3 (99:1), DOPC:GD1a (99:1), DOPC:GSL (99:1), DOPC:PIP2 (99:1), and total brain extract BBB etc by dissolving the lipids in chloroform and/or methanol in an appropriate mol:mol ratio in a 1.5 mL glass amber vials. To produce a thin film, the lipid solution was dried under HP N2 for 1 minute. It was then dried in vacuum for an additional 1 hour. The dried lipid films were then rehydrated in HEPES buffer, pH 7.4 and vortexed for a period of 30-60 s. Next, the lipid suspensions were extruded 11 times through a 100 nm polycarbonate filter using a mini-extruder (Avanti Polar Lipids) to form large unilamellar vesicles (LUV) that were then diluted to final concentration of 0.25 mg/mL and stored at 4 °C for further use. For fluorescence-based studies, additional 0.01 mol% of fluorescently labelled lipids such as ATTO655-PE, ATTO532-PE, BODIPY-GM1 etc were co-mixed with the aforementioned lipid organic solution mixes prior to drying.

2.2 Lipid bilayer preparation: Symmetric and asymmetric lipid bilayers over solid substrate such as glass, mica and over micropore cavity gold and PDMS substrates were prepared using a combination of Langmuir-Blodgett (LB) transfer followed by vesicle fusion (VF) method (LB-VF). Prior to LB transfer, the substrate was submerged beneath a well-packed lipid monolayers that formed at air/water interface using a LB trough (Model KN2006, KSV-NIMA technology). To form a well-packed monolayer, ~50µL from 1mg/mL lipid dissolved in chloroform solution was added dropwise to the LB trough and chloroform was allowed to evaporate. The monolayers were transferred at a highly condensed surface pressure of 33 mN/m by the vertical withdrawal of submerged substrate at a speed of 5 mm/min. To form lipid bilayer, the monolayer-coated substrate was brought into the contact of LUV solution for at least 1 hour for fusion to occur, and then washed with HEPES buffer to remove any unfused vesicles without exposing it to air.

2.3 Substrate fabrication and pre-treatment: Glass coverslip (20mm × 20mm × 0.18mm, length × bredth × thickness) and freshly cleaved mica substrates were washed with acetone, ethanol and milli-Q water to remove any impurities, dried under high pure N_2, and then O_2 plasma treated for 5 minutes to make the surface hydrophilic. Hemispherical micropore imprinted gold (each pore size 1µm diameter) and PDMS (each pore-size~2µm) substrate were prepared from the soft-lithography method according to our established method and also provided in supplementary information. Prior to buffer filling, the PDMS cavities are O_2 plasma treated whereas gold substrate's intestinal top surface was modified with 6-mercaptohexanol to render the substrate hydrophilic.

2.4 Electrochemical impedance spectroscopy: Non-Faradaic electrochemical impedance spectroscopy (EIS) was performed using a CH Instrument model 760E. A three-electrode cell arrangement was used, using platinum wire as an auxiliary, an Ag/AgCl (1M KCl) as a reference, and a gold microcavity array as the working electrode. EIS was measured over a frequency range of 10^5 Hz

to 0.05 Hz with an AC modulation amplitude of 0.01 V at a potential bias of 0 V (vs Ag/AgCl). All measurements were performed in a glass cell (~4 mL volume) in HEPES buffer (pH 7.4) at 22±°C. In the absence of peptide, all symmetric and asymmetric MSLB's admittance remain stable for 24 hours with initial fluctuation that were seen within 1-2 hours due to ion equilibration from bulk to the cavity interior through bilayer membrane. Once the EIS signal is equilibrated (i.e., after 2 hours of EIS recording following bilayer preparation), 1μM $A\beta_{1-42}$ in its monomeric form was added to the electrochemical cell and EIS measurement were further performed for 22 hours. An equivalent circuit model (ECM) was used to fit the measured AC impedance data using ZView software (version:3.4e, Scribner Associates, Inc) to estimate the membrane resistivity and capacitance, as reported previously. A Constant Phase Element (CPE) is used in the equivalent circuit instead of pure capacitors to account for surface defects on both the electrode surface and the lipid bilayer. The impedance of a CPE is given by $Z_{CPE} = Q^{-1}(j\omega)^{-\beta}$ where Q is the magnitude of the capacitance of the CPE, ω is the angular frequency, and the exponent β is a real number between 1 and 0 (the closer β approaches 1, the more ideal the capacitive behavior of the CPE). In all our measurements, the CPE exponent β for membrane and cavity array was found to be 0.94±0.2 and 0.5±0.04 respectively. The temporal changes of membrane admittance upon $A\beta_{1-42}$ binding are reported herein as the relative changes (ΔR and ΔQ) values with respect to the membrane's equilibrated value.

2.5 Atomic force microscopy: Atomic force microscopy (AFM) imaging of lipid bilayers before and after $A\beta_{1-42}$ incubation at different time intervals were carried out using the Veeco Bioscope II system (Nanotec House, Cambridge) coupled with a Zeiss Axiovert inverted optical microscope IX70. Topographic AFM images of bilayer were imaged under liquid, in a homemade liquid cell containing ~0.5 mL HEPES buffer in tapping mode, using silicon nitride cantilevers PNP-TR-20 (NANO WORLD) with a nominal force constant of 0.32 N/m and a tip radius of 20 nm. During image acquisition, the resonance frequency in buffer was kept as low as possible, and the scan rate was kept at 0.5 Hz. For AFM studies, lipid bilayers were prepared on freshly cleaved hydrophilic mica substrate using the LB-VF method. All AFM images were analyzed using Nanoscope 7.30 software, and the whole images were plane fitted with a 1^{st} order polynomial.

2.6 Fluorescence lifetime microscopy imaging and fluorescence correlation spectroscopy: Fluorescence lifetime microscopy imaging (FLIM) and point fluorescence correlation spectroscopy (FLCS) studies were carried out on a Microtime 200 system (PicoQuant GmBH, Germany) that configured with an FCS module, dual SPD detection unit, time-correlated single photon counting (TCSPC), and an Olympus X1-71 inverted microscope with an Olympus UPlan SApo 60x/1.2 water immersion objective. The fluorescent labelled Aβ555 or lipid (ATTO532-PE, BODIPY-GM1) and fluorescent labelled lipid, ATTO655-PE were stimulated using pulsed picosecond lasers from Toptica

(Picoquant) at 532 nm laser PicoTA and 640 nm LDH-P-C-640B Picoquant, respectively. The two lasers are guided to the main unit by a single mode optical fibre, which gives a homogenous Gaussian profile for both excitations. The lasers were pulsed at 20 MHz, with intervals of 50 ns. The emitted fluorescence was collected using the microscope objective, and backscattered light was blocked using a dichroic mirror z532/635rpc, and the signal was cleaned using HQ550lp AHF/Chroma filters for 532 nm and HQ670lp AHF/Chroma filters for 640 nm. x MPD's (Picoquant) single photon avalanche diode (SPAD) was used to detect fluorescence. The time-correlated single photon counting system, TCSPC (PicoHarp 300 from Picoquant) allowed for simultaneous measurement of lifespan in nanoseconds and diffusion time in milliseconds. Using TCSPC, we were able to filter out any after-pulsing contribution, suppress scattered light, parasitic signals, and background, while also calculating the fluorescence lifetime of the lipid/peptide probes in situ.

Single point FLCS measurements from the spatial position in the bilayer 2D plane were recorded for 30s by positioning the observation confocal volume. The time-dependent fluctuations of the fluorescence intensity were recorded and then autocorrelated using SymphoTime (SPT64) software version 2.2 (PicoQuant) to obtain an autocorrelation function (ACF). The ACF trace, G(t) versus time, t, plots were then fit to a two-dimensional (2D) diffusion model Eq. (1) using Origin software (v22) to obtain the transit time of tracer molecules of interest at 2D;

$$G(t) = \frac{1}{N}\frac{1}{1+(t/\tau_D)^{\alpha}} \qquad (1)$$

where, τ_D is the transit time, N is the average lipid probe number, and α is the anomaly coefficient. $G(t)$ is autocorrelation measure of the self-similarity of a signal in time, i.e., the overlap of a signal with itself at various lag time. From the fitting the τ_D values were evaluated and accordingly, the mobility (diffusion coefficient) of fluorescently labelled lipid and/or peptide can be obtained by Eq. (2);

$$D = \frac{r_0^2}{4\tau_D} \qquad (2)$$

where r_0 is the observation beam waist diameter typically obtained from calibration of a standard dye diffusing in 3D with a known diffusion coefficient value. The confocal volumes differ depending on the excitation laser; the confocal volumes for 532nm and 640nm excitation were calibrated using Rhodamine 6G and ATTO655-carboxylic acid nM water solution, for which the diffusion coefficients are known. Some of the observed ACF traces, particularly those from peptide diffusion, include two diffusion time components, which were evaluated by fitting the ACF with Eq. (3);

$$G(t) = \frac{1}{N}\left[\frac{1}{1+(t/\tau_{D1})^{\alpha 1}} + \frac{1-c}{1+(t/\tau_{D2})^{\alpha 2}}\right] \qquad (3)$$

Where τ_{D1} and τ_{D2} are the diffusing time of fast- and slow-moving species. To visualize the membrane leaflet using FLIM, and to obtain the translational lipid mobility using FLCS, the bilayer leaflets were selectively doped with fluorescent lipid marker. To visualize peptide association at the membrane surface and its diffusion, 50 nM Hylyte Aβ555 was pre-mixed with 950 nM of unlabelled $A\beta_{1-42}$ and added exogenously to the membrane surface in a thin buffer chamber. All measurements were carried out in HEPES buffer at 22±1°C in triplicate.

3. Results

3.1 $A\beta_{1-42}$ monomer exhibits stronger binding and aggregation at negatively charged membrane over zwitterionic membrane.

3.1.1 Electrochemical impedance spectroscopy and atomic force microscopy imaging display anionic membrane pore- and peptide aggregate-formation. To elucidate the molecular mechanism of membrane mediated $A\beta_{1-42}$ aggregation, we initially employed non-Faradaic electrochemical impedance spectroscopy (EIS) as a label-free and extremely sensitive. method on a microcavity suspended lipid bilayer (MSLB) to deduce the characteristics of the membrane before and after its interaction with monomeric $A\beta_{1-42}$. In these studies, the membrane was spanned over microcavity imprinted gold cavity array (Scheme 1a) electrode (each pore diameter 1μm and pore depth 0.5 μm) prepared via Langmuir-Blodgett and vesicle fusion (LB-VS) method, as described previously.[39,40] The MSLB platform features a microcavity pore array that provides water reservoirs at each lipid leaflet interface, hence preventing any loss of activity or peptide assembly due to substrate effects. The layer-by-layer fabrication method facilitates the precise incorporation of asymmetry into the MSLB structure, exhibiting transversal fluidity akin to that of free-standing cell membrane. The relevant parameters from EIS are membrane capacitance and resistance, which reflect how the peptide affects the modulation of membrane admittance characteristics over time. Typically, non-Faradaic EIS utilizes alternating current (AC) at varying frequencies to measure the impedance (resistance) to ionic conduction through a lipid bilayer and to analyze the capacitance properties of the bilayer, which are associated with the membrane's thickness. Admittance is inversely related to impedance. Membrane thickening, characterized by a reduction in capacitance and an increase in impedance or resistance, may occur due to the aggregation of macromolecules at the membrane interface, resulting in layer development without compromising membrane integrity. Conversely, an increase in membrane capacitance indicates membrane thinning or damage to the membrane. An increase in membrane admittance, characterized by enhanced ion conduction or reduced impedance, with negligible changes in membrane capacitance, indicates the emergence of ion channels or pore formation in the membrane.[26] These parameters are obtained by fitting the EIS data using an equivalent circuit model (ECM) as shown in Scheme 1a.

Figures 1a and b show the real-time changes to membrane relative resistance (ΔR, filled symbols) and constant phase element, CPE capacitance (ΔQ, open symbols) for symmetric DOPC//DOPC (black) and asymmetric DOPC//DOPC:PIP2 (99:1 mol/mol) (red) microcavity pore suspended lipid bilayers (MSLBs). Data is given relative to the bilayer's equilibrated impedance (horizontal dotted line, panel a and b) following incubation with monomeric 1μM $A\beta_{1-42}$. At 1μM, the $A\beta_{1-42}$ the peptide remains monomeric in nature, independently confirmed from single molecule-based fluorescence correlation spectroscopy (FCS) (Fig. S1a,b, Supporting Information (SI)). The EIS response of zwitterionic DOPC bilayer over 20 hours incubation with 1μM $A\beta_{1-42}$ showed a modest increase in admittance only after 12 hours suggesting any binding and assembly of $A\beta_{1-42}$ at the membrane is weak (Fig. 1a,b, black square). In contrast, negatively charged DOPC:PIP2 bilayer shows a systematic decrease in resistance over the first 4 hour, that equilibrates (4-8 hours) and then proceeds to increase after 8 hours (Fig. 1a, filled red circle). Capacitance follows an inverse trend to resistance (Fig.1a, open red circle). Considering that capacitance is inversely correlated with membrane thickness[39,41], the combined data on capacitance and resistance indicates that the peptide initially induces membrane thinning/pore-formation, which is then followed by membrane thickening due to the development of peptide aggregates during prolonged incubation. This interpretation is corroborated by atomic force microscopy (AFM) imaging of mica supported lipid bilayers under the same conditions, demonstrating that 1μM $A\beta_{1-42}$ triggered pore formation in negatively charged DOPC:PIP2 membranes after approximately 1 hour of incubation, with aggregate formation occurring after prolonged incubation (~18 hours) (Fig. 1d). From topography and corresponding height profile analysis, it is evident that some of the $A\beta_{1-42}$ aggregates are deeply buried within the DOPC:PIP2 membrane (Fig. 1d). When compared to DOPC:PIP2, no such aggregates are developed at zwitterionic DOPC membrane (Fig. 1c).

3.1.2 Fluorescence lifetime imaging and fluorescence lifetime correlation spectroscopy reveal enhanced interaction of $A\beta_{1-42}$ with anionic membrane. Fluorescence lifetime imaging microscopy (FLIM) is employed due of its sensitivity to molecular environments and conformational alterations, leveraging the property of fluorescence lifetime. The lifetime histogram plots, from the FLIM image can offer specific insights regarding peptide-membrane binding at different incubation time point. Fluorescence correlation spectroscopy (FCS) in lifetime mode utilizes variations in fluorescence intensity decays to distinguish contributions from different fluorophore populations to the FCS signal. It is an effective method for enhancing the quality of FCS data by eliminating noise and distortion from scattered excitation light, detector thermal noise, and detector after pulsing.[42] In this study, we performed fluorescence lifetime imaging (FLIM) and fluorescence correlation spectroscopy (FCS) in lifetime mode at different time intervals of peptide binding to elucidate how the interaction of $A\beta_{1-42}$ with zwitterionic DOPC and negatively charged DOPC:PIP2 membranes provided insights beyond simple localization, including diffusional mobility, peptide clustering and interactions, as well as the

effects of the molecular environment on membrane homogeneity FLIM images of the glass supported lipid bilayer were collected at an excitation wavelength of 640 nm, where the outer leaflet of bilayer was selectively doped with fluorescent lipid marker, ATTO655-PE (0.01 mol%). Zwitterionic ATTO dyes are relatively hydrophilic, preventing their transversal migration to opposing leaflets[39] within the experimental timescale used here. A 532 nm excitation laser was used to facilitate imaging from the peptide channel, where a 50 nM of Hilyt555 $A\beta_{1-42}$ was pre-mixed with 950 nM unlabelled $A\beta_{1-42}$ (henceforth called as Aβ555) and this mixture was added to the bilayer contact buffer. The FLIM image was utilized to assess the intrinsic molecular brightness (MB, the number of emitted photons per second per molecule) of both fluorescently labelled lipid and peptide at the bilayer plane, in order to evaluate the degree of membrane damage, organization, or peptide association during various time point of peptide-membrane interaction. FLIM image of the membranes collected 1 hour post incubation with $A\beta_{1-42}$ further confirmed greater but uniform association of the peptide to the anionic DOPC:PIP2 membrane (Fig. 1g, bottom middle panel) compared with neutral DOPC-only membrane (Fig. 1e bottom middle panel). After 18 hours, the FLIM signal or MB from the DOPC:PIP2 membrane channel weakens considerably by ca. 30 to 40%, whereas MB from the peptide channel, the signal increases (Fig. 1g, right panel). This suggests membrane poration and micron scale peptide aggregate formation, which is consistent with EIS and AFM data. By comparison, at DOPC only membrane, peptide interaction is absent at early stage of $A\beta_{1-42}$ incubation (1 hour), as evident from no FLIM signal from peptide channel at the DOPC membrane (Fig. 1e, bottom middle panel). Though, a few nanoscale peptide aggregates can be seen after 18 hours (indicated by the arrow, bottom right panel of Fig. 1e) of peptide binding.

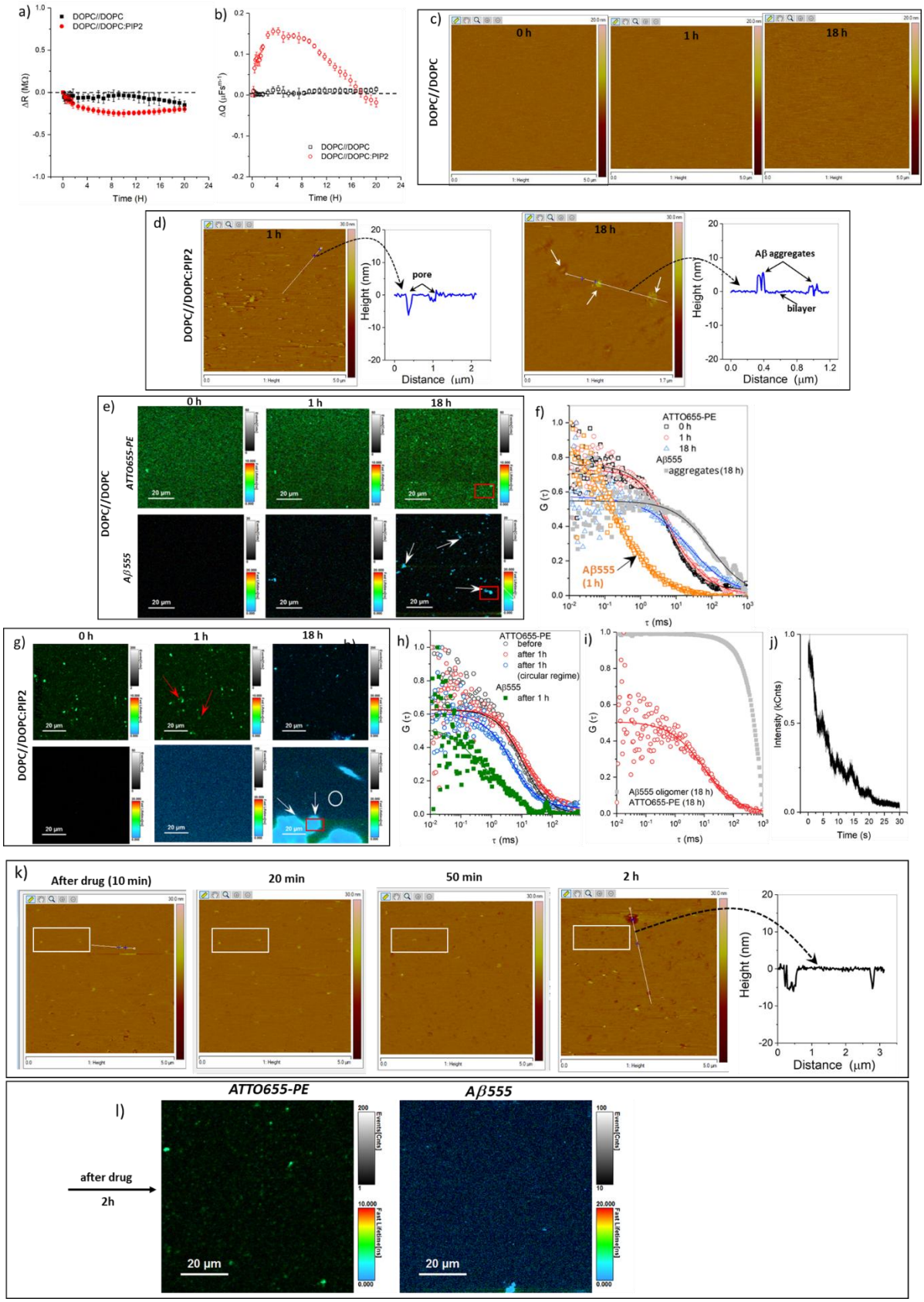


Figure 1. Temporal changes in relative a) resistance (filled symbol) and b) capacitance (open symbol) of DOPC (black) and DOPC:PIP2 (red) MSLB from equilibrated membrane electrochemical impedance data (horizontal

dotted line near zero) upon incubation with 1μM $A\beta_{1-42}$. The DOPC membrane was assembled over hemispherical 1 μm microcavity imprinted electrode of physical dimension (1 cm×1 cm). EIS measurements were performed in contact with HEPES buffer electrolytes (pH 7.4) at 20 °C using gold microcavity suspended bilayer as working electrode, Ag/AgCl (1 M KCl) as reference electrode and Pt coil as counter electrode. Measurements were taken at an AC perturbation amplitude of 10 mV with DC bias potentials 0 V (vs. Ag/AgCl), over the frequency range from 0.05 to 10^5 Hz. Prior to peptide addition, the membranes were equilibrated (dotted line, panel a and b). The data are presented as the mean of N = 3, and the error bars are ±SD. (c) Illustrate the representative topographic AFM images of symmetric DOPC membrane imaged under buffer prepared over freshly cleaved mica before (0h) and after 1h and 18h of incubation with 1μM $A\beta_{1-42}$. The scale bar in each image is 5μm×5μm. (d) AFM image of asymmetric DOPC:PIP2 image after 1h and 18 h of $A\beta_{1-42}$ binding along with the line profile analysis shown next to the image indicated by curved arrow. Temporal evolution FLIM images of lipidic channels (top) and peptide channels (bottom) obtained from e) DOPC and g) DOPC:PIP2 lipid bilayers prepared over O_2 plasma treated glass substrate before (0 h) and after incubation with 1μM $A\beta_{1-42}$ at different time intervals (1h and 18 h). The scale bar of each FLIM images was 20μm. All bilayers were prepared over gold, mica and glass substrates using LB-VF method. All imaging measurements were carried out using a home-made cell containing ~0.5 mL of HEPES buffer. f) Representative autocorrelation function (ACF) traces of the lipid marker ATTO655-PE (open symbol) before (0h, open black), after 1h (open red), and after 18 h (open blue) of peptide incubation in DOPC bilayer. The ACF of monomeric $A\beta_{1-42}$ mobility in solution and DOPC membrane bound $A\beta_{1-42}$ aggregates are depicted with open orange and filled grey circles respectively in panel f. h) Illustrate ACFs of lipid mobility in DOPC:PIP2 (99:1) bilayer; before (0h, open black) and after 1 h (open red and open blue) of peptide incubation. The membrane-bound peptide ACF after 1 h is depicted in filled olive in panel h. i) The ACFs of both lipid (open red) and peptide (filled grey) after 18 hours peptide binding to DOPC:PIP2 are also presented. The translational diffusion coefficients of lipid and peptide were obtained by fitting the ACF using a 2D diffusion model fit Eq. (1), whereas the monomeric $A\beta_{1-42}$ in solution was fitted to a 3D diffusion model as defined in Eq. (S1), SI. j) The intensity-time trace obtained from the DOPC:PIP2 membrane bound peptide aggregate regime is highlighted within the red rectangular box in panel g. k) Topography and l) FLIM image showing the disappearance of membrane bound $A\beta_{1-42}$ aggregates upon treatment with synergistic drugs, imipramine (10 μM) and fluoxetine (1 μM).

Single point fluorescence correlation spectroscopy (FCS) in lifetime mode was next carried out to assess the extent of lipid-peptide interaction by independently sampling lipid and peptide mobility at different incubation time points. The intensity-intensity fluorescence autocorrelation function (ACF), G (τ) was computed from the observed fluctuations of the tracer fluorophore molecules transiting across the confocal volume in two-dimension plotted against the lag time (τ). The ACF data were fit using equation (1) and the diffusivity, D values obtained from equation (2) (see experimental methods). A modest reduction in two-dimensional (2D) lipid diffusivity was noted, from 5.1±0.4 $\mu m^2/s$ (cf. ACF in Fig. 1f, black (before)) to 4.2±0.3 $\mu m^2/s$ (Fig. 1f, red) following $A\beta_{1-42}$ incubation with DOPC for 1 hour; however, the peptide diffusion remains within error from that of the bulk solution, which has a mean

diffusivity of 76±8 $\mu m^2/s$ and an anomalous parameter, α=1. This suggests that the peptide remains largely unbound to DOPC membrane at early times. Following 18 hours of incubation, the membrane diffusivity is reduced to 1.7±0.1 $\mu m^2/s$ (ACF in blue, Fig. 1f) and 2D peptide diffusivity of 0.3±0.06 $\mu m^2/s$ (ACF in grey, Fig. 1h) is estimated from the spatially distinct nanoscale peptide aggregates (red rectangle box in panel 1e) with an associated anomaly coefficient, α of 0.85±0.1. This indicates that after prolong incubation, nanoscale self-aggregated peptides formed (as evident from thioflavin-T assay, Fig. S1c, SI) in solution may have adhered to the zwitterionic DOPC membrane while increasing global membrane viscosity. In contrast, the 2D peptide diffusion after approx. 1 hour incubation with DOPC:PIP2 membrane decreased to 62±5 $\mu m^2/s$ (cf. ACF in olive, Fig. 1h) compared to bulk diffusion, (~ 78 $\mu m^2/s$), suggesting that $A\beta_{1-42}$ binds weakly to the DOPC:PIP2 membrane surface while remaining monomeric. The diffusion coefficient of the ATTO655-PE lipid marker in the pristine DOPC:PIP2 bilayer was 4.7±0.17 $\mu m^2/s$, as shown by the black ACF in Fig. 1h, with α=1. After 1 hour of incubation with the peptide, the diffusivity becomes biphasic, measured as 3.0±0.11 $\mu m^2/s$ (cf. ACF in red, Fig. 1h) with α= 0.78, and 6.25±0.3 $\mu m^2/s$ (ACF in blue, Fig. 1h) with α=1. On careful inspection, the slower lipid diffusion (D = 3.0±0.11 $\mu m^2/s$) occurs from the overall membrane surface while the faster diffusion (D = 6.25±0.3 $\mu m^2/s$) arises from circular domains that show greater emission intensity across the membranes (red arrow in middle panel of Fig. 1g). It is worth noting that the size of these fluidic microscopic domains increases laterally when the peptide incubation window is extended further to 3–4 hours (Fig. S2a, SI). After 18 hours, the fluidic microdomains disappear, leading to a homogeneous membrane, which results in an overall decrease in MB in the membrane channel and an increase in lipid diffusion (D = 3.74±0.22 $\mu m^2/s$, ACF in red, Fig. 1i), possibly due to extensive pore-formation. At this late time point, the peptide has aggregated, as seen in the FLIM image (as colonies of circular aggregates from peptide channel, cf. white arrow, Fig. 1g), and remains immobile within the limitations of the experiment (ACF in grey Fig. 1i), as no ACFs could be obtained due to photobleaching of the slowly diffusing species depicted in the intensity-time trace in Fig. 1j.

3.1.3 Disassembly of anionic membrane mediated $A\beta_{1-42}$ aggregates by repurposed drugs. From the AFM and FLIM imaging studies above, micron scale circular $A\beta_{1-42}$ aggregates develop via a membrane mediated assembly of $A\beta_{1-42}$ at the anionic DOPC:PIP2 membrane following 18 hours of incubation (Figure 1 d, g). Thus, using these markers, we investigated small molecule drug synergism as an approach to disassemble these membrane mediated peptide aggregates and to halt the progression of aggregates to fibrils, as potential strategies to discover AD therapeutics. We identified a synergistic combination of the two antidepressants fluoxetine (1 μM) and imipramine (10 μM) (see chemical structure in Scheme 1 (h) and (i) respectively), both within physiological limits[43], that effectively eliminate membrane-mediated $A\beta_{1-42}$ aggregates. The rationale behind choosing such two drugs is that they are both CNS+ drugs[34] that can passively permeate the neuronal membrane without causing

membrane damage. We recently discovered that imipramine can passively permeate a range of biomimetic membranes, including zwitterionic DOPC and the reminiscent of blood-brain-barrier(BBB).[44] Upon administration of imipramine and fluoxetine, these peptide aggregates disassembled from the membrane surface within 1 hour, leaving the membrane porous, as evidenced by temporal AFM imaging (highlighted in rectangular box, Fig. 1k) and the subsequent FLIM image (Fig. 1l). When monomeric $A\beta_{1-42}$ is preincubated with these drugs and subsequently added to the DOPC:PIP2 bilayer, the binding and assembly pathways described by the EIS trends noted in Fig. 1 a and b are absent. Instead, only a modest decrease in admittance (Fig. S2b,c, SI) is observed, indicating the drug effectively inhibits membrane mediated aggregation of $A\beta_{1-42}$ as well.

The drug induced the disassembly of the membrane-mediated peptide aggregates, which was further tested using a different negatively charged asymmetric DOPC:DOPS (90:10) membrane. We recently described that a carpet-like layered $A\beta_{1-42}$ aggregates developed post 18 hours binding of $A\beta_{1-42}$ to the asymmetric DOPC:DOPS membrane.[26] In our previous work, we did not examine drug interactions; hence, this analysis was conducted here for comparative purposes. As described previously, the incubation of 1μM $A\beta_{1-42}$ with a DOPC:DOPS bilayer for 18 hours lead to the formation of layered-like peptide aggregates (Fig. S3a, SI). A systematic strategy of drug addition was employed to further substantiate the mechanistic aspect of the drug synergism approach. The administration of 1 μM fluoxetine alone lead to an increase in membrane-bound $A\beta_{1-42}$ aggregates height from the membrane surface without the elimination of peptide aggregates even up to 4 hours. Upon the subsequent addition of 10 μM imipramine, while fluoxetine remained in contact with the bilayer, time-lapsed imaging shows the progressive disappearance of $A\beta_{1-42}$ layered-like aggregates from the membrane surface within 90 minutes. This was quantitatively confirmed by the decrease in height profile analyses shown in the bottom panel of Figure S3a (SI). Notably, when administered alone, imipramine did not result in aggregate elimination (data not shown). Currently, there is insufficient knowledge regarding the underlying mechanism by which each drug dismantles the peptide aggregates facilitated by the membrane. The core/central aromatic hydrophobic amino acid side chains involved in peptide aggregate formation[45] may exhibit enhanced recognition of fluoxetine, potentially elucidating the observed phenomena. Consequently, imipramine further facilitates the disintegration of aggregates through advantageous $\pi-\pi$ interactions between aromatic ring of imipramine and amyloid beta side chain. The disassembly of peptide aggregates from DOPC:DOPS membrane was strongly corroborated by the FLIM imaging shown in Figure S3b (SI). The direct interaction of the drugs with the membrane-bound $A\beta_{1-42}$ aggregates at the DOPC:DOPS membrane is evident from the decreased admittance (Fig. S3c, SI), whereas the admittance increased upon incubation of the drugs at the peptide-free pristine membrane (Fig. S3d, SI) due to passive drug permeation.[44] In a control experiment, when monomeric $A\beta_{1-42}$ is preincubated with fluoxetine and imipramine, and this solution is subsequently incubated with

the DOPC:DOPS membrane for 18 hours, we did not observe any carpet-like $A\beta_{1-42}$ aggregates by AFM. Instead, the membrane became moderately porous (Fig. S3e, SI). These observations further suggest that the studied drugs (imipramine and fluoxetine in synergy) not only disassemble the membrane-mediated peptide aggregation but also possess the ability to arrest peptide aggregation.

3.2 $A\beta_{1-42}$ monomer exhibits different cooperative binding and assembly to GM1 receptors

Considering the prevalence of gangliosides in neuronal membranes, and their asymmetric distribution, we then investigated the impact of negatively charged N-acetylneuraminic acid (Neu5Ac) in the GM1 receptor on $A\beta_{1-42}$ aggregation and its interaction with a DOPC membrane interface. Since gangliosides are confined to the outer surface of neuronal membranes,[46,47] we prepared an asymmetric DOPC//DOPC:GM1 membrane, with the lower/proximal leaflet comprised of 100 mol% DOPC and the upper/distal leaflet comprised of DOPC:GM1(99:1) (mol/mol). The establishment of an asymmetric DOPC:GM1 bilayer over gold microcavity imprinted array was validated by FLIM. FLIM images were collected from two spectroscopically well resolved fluorescent markers used to label each leaflet of bilayer individually; the proximal DOPC layer was fluorescently labelled with 0.05 mol% ATTO655-PE and the distal DOPC:GM1(99:1) leaflet was labelled with 0.05 mol% BODIPY-GM1 (Fig. S4, SI). The interaction of $A\beta_{1-42}$ with DOPC:GM1 asymmetric membrane in real-time was initially assessed by EIS. Figure 2a shows the temporal impedance changes to DOPC:GM1 membrane following incubation with monomeric 1 μM $A\beta_{1-42}$. Incubation with $A\beta_{1-42}$ results in a modest resistance decrease that saturates at ca. 2 hours. After ca. 4 hours, resistance proceeds to increase further until it exceeds the original equilibrated bilayer resistance (dotted line, Fig. 2a) equilibrating at ca 8 hours and then remains stable beyond 16 hours (Fig. 2a, top panel). Compared to pristine DOPC membrane (cf. Fig. 1a, vide infra), the magnitude of the impedance changes indicate strong binding is occurring between $A\beta_{1-42}$ and GM1 and the aggregation is time dependent. The corresponding capacitance changes (Fig. 3a, bottom panel b), show an opposing trend, i.e., with an initial modest rise in capacitance on peptide incubation that equilibrates and gradually decreases until 14-16 h. The decrease in capacitance after 2 hours of $A\beta_{1-42}$ binding is taken to indicate membrane thickening attributed to peptide aggregation. However, given the lower magnitude of decrease in resistance and increase in capacitance at early stages (~ 1 h) of peptide binding, compared to DOPC:PIP2, transmembrane pore-formation is deemed very unlikely in this case. Instead, impedance changes are attributed to reorganisation of the receptor GM1 clusters on $A\beta_{1-42}$ association with GM1. This is confirmed by AFM, where direct interaction of GM1 nanocluster (protruding ~1.2 nm height from the membrane surface) before and after $A\beta_{1-42}$ binding is captured (cf. rectangular box in Fig. 2b and corresponding height profile). Formation of GM1 clusters at membrane surfaces have been described at numerous model membranes and is facilitated by sugar-sugar intermolecular hydrogen bonding [48–51]. Circular submicron scale peptide aggregate formation at DOPC:GM1 surface was also captured post 18 hours of incubation (Fig. 2b, right panel) by using

AFM. Line profile analyses show that peptide aggregates have a lateral diameter of ca. 350±10 nm and protrude at a height ca. 5 nm from the bilayer surface.

Subsequently, we conducted FLIM imaging, a sophisticated technique for differentiating the distinct molecular environments of lipid and peptide fluorophores during their interactions. FLIM typically quantifies the duration a fluorophore remains in an excited state prior to photon emission, and identifies chemical changes of fluorophores that are not discernible by spectral methods alone. In addition to visually inspecting the FLIM image, we plotted intensity versus lifetime histograms from both the lipid and peptide fast FLIM image channels to observe any alterations in the respective lifetime probes due to peptide-membrane interactions at different time point. All our FLIM imaging studies were carried out on a glass supported asymmetric DOPC:GM1 membrane. Prior to the incubation with peptide, the lipid channel (ATTO655-PE) appears homogeneous, and we confirmed no potentially interfering signal in the Aβ555 peptide channel (0h, Fig. 2c). After 1 hour incubation with Aβ555, the membrane becomes moderately heterogeneous with an accompanied modest increase in ATTO655-PE molecular brightness (MB), reflected in both FLIM image and occurrence versus probe lifetime amplitude histogram plot respectively. The peptide channel of FLIM image shows that Aβ555 has a greater association with the DOPC:GM1 membrane when compared to pristine DOPC membrane as shown in Fig. 1e (*vide infra*). Additionally, the peptide probe lifetime amplitude distribution becomes biphasic (panel c, right). Spherical peptide aggregates have a short lifetime (mean value ~ 1 ns) with a low but broad occurrence amplitude (0.06×10^6), while from the uniform peptide coverage has a relatively high mean lifetime (1.81 ns) with a narrow but higher occurrence amplitude (7.6×10^6). After 18 hours of incubation, the density and the size of the spherical peptide aggregates increase. Furthermore, after 18 hours, from the membrane channel, we observe emergence of lipidic nanodomains (highlighted in rectangular box, Fig. 2c). Some of these lipidic nanodomains colocalize with the $A\beta_{1\text{-}42}$ spherical aggregates (highlighted in white square box), possibly due to tightly peptide bound annular lipids; however, other distinct, brighter lipidic domains also form, which appear to be liquid disordered domains (highlighted in orange triangle, panel c), as confirmed by using spatially resolved FCS (data not shown).

FCS investigations were next conducted to investigate the diffusion dynamics of lipids and peptides, as well as any alterations happening during peptide-membrane interplay interactions.. Prior to the addition of peptide, the lipid diffusivity at the asymmetric DOPC:GM1 membrane was measured as 3.8±0.14 $\mu m^2/s$ (cf. ACF in black symbol, Fig. 3d). This value is lower than the diffusivity of the pristine DOPC membrane (5.1±0.4 $\mu m^2/s$).[52] After incubating the peptide for 1 hour, we observed a bimodal lipid diffusivity. The slower component (ACF represented by the red symbol, Fig. 2d) had a diffusivity value of 0.89±0.06 $\mu m^2/s$, which was obtained from the spatially defined $A\beta_{1\text{-}42}$ aggregated circular

regimes. The faster component (blue symbol, Fig. 3d) had a diffusivity value of 5.6±0.11 $\mu m^2/s$, which was consistent across the remaining membrane areas. The anomalous exponent, α, consistently approached a value of 1, indicating Brownian lipid diffusion in all cases. Following a further 18-hours incubation, lipid diffusivity at the spatially distinct peptide aggregated regions further decreased to 0.43±0.04 $\mu m^2/s$ (red symbol, Fig. 2e) with α of 0.64. This indicates a non-Brownian sub-diffusion regime that is attributed to barriers created by the $A\beta_{1-42}$ aggregates. The diffusivity obtained from the rest of the membrane outside these regions was also reduced to 1.78±0.11 $\mu m^2/s$, with an α value of 0.78, possibly due to sub-diffraction limited dimensioned aggregates that impede lipid diffusion outside of the large aggregates. A reliable peptide ACF from either circular or broader membrane, where a uniform peptide emission signal is observable, was not obtained due to signal photobleaching (Figure S5, SI) during FCS acquisition, which aligns with extensive binding and aggregation of the peptide at the membrane interface.

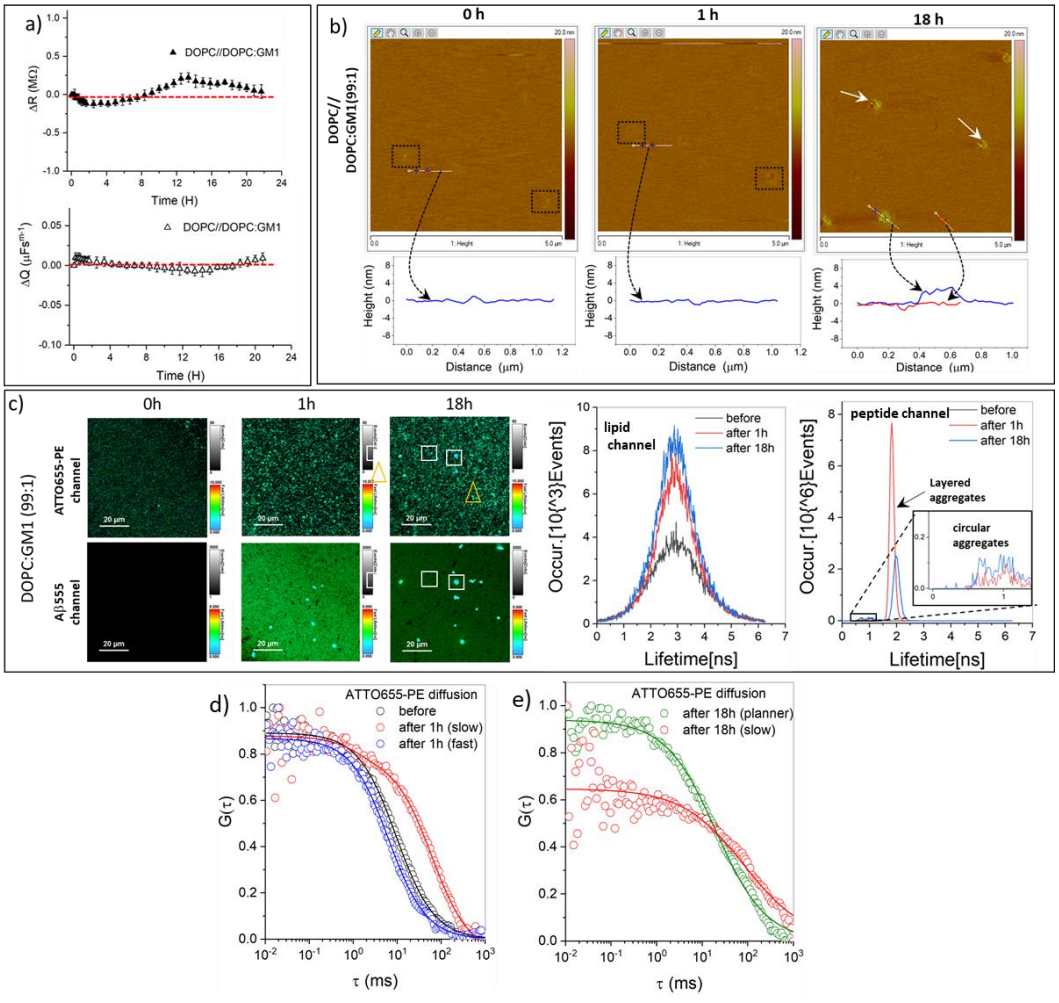


Figure 2. a) Illustrate temporal changes in asymmetric DOPC:GM1 (99:1) MSLB membrane's resistance (*top*) and capacitance (*bottom*) upon binding with 1μM $A\beta_{1\text{-}42.}$ Error bars represent standard error of the mean (N = 3). b) Topographic AFM images (top panel) of DOPC:GM1 membrane supported over mica before (0h) and after 1h and 18h incubation with incubation with $A\beta_{1\text{-}42}$. The GM1 nanoclusters regimes are highlighted in rectangular black box and the $A\beta_{1\text{-}42}$ aggregate structures are indicated by white arrow. Bottom panel of b indicates the line profile corresponding to the spatial regimes of bilayer indicated by black arrow. The image size was 5μm×5μm. c) FLIM images obtained from the glass supported DOPC:GM1 asymmetric membrane before (0h) and after (1h and 18h) $A\beta_{1\text{-}42}$ binding. The outer leaflet of the lipid membrane is labelled with ATTO655-PE and the peptide is labelled with Hylyte555. The FLIM images shown in top and bottom panel of c are taken sequentially from the lipid (λ_{ex} = 640 nm) and peptide ((λ_{ex} = 532 nm) channel respectively. The histogram plots shown to the right panel of c are the corresponding lifetime signal from the FLIM images taken from lipid and peptide channel at different incubation time intervals (black: 0 h; red: 1h; blue 18h). d) The ACF trace obtained from lipid marker, before and after 1h of $A\beta_{1\text{-}42.}$ incubation at two different spatial regimes (marked as peptide's spherical aggregated regime (slow) and layered-like panner regime (fast)) are shown in open symbols black, red and blue respectively. e) ACF of lipid markers after 18h incubation from planner (green) and aggregated (red) regimes. The solid lines in the panels d and e are the fit using 2D diffusion model Eq. (1).

3.2.1 GM1 mediated amyloid beta aggregates impacted hindered lipid mobility across each leaflet. To understand how exofacial binding of the $A\beta_{1\text{-}42.}$ peptide affects the diffusion of receptor GM1 in the outer leaflet and its influence on lipid diffusion in the lower leaflet, we labelled the individual leaflets of the DOPC:GM1 asymmetric membrane with spectrally resolved lipidic fluorophores. Such leaflet-by-leaflet membrane sampling was previously reported in pore-forming proteins[53]- and antimicrobial peptides[54]-membrane interactions and can provide insight into the extent of action/depth of penetration of protein or peptide across the bilayer. Here, the proximal DOPC leaflet was fluorescently doped with ATTO655-PE (0.01 mol%) and the distal DOPC:GM1 leaflet with BODIPY-GM1 (0.01 mol%), each layer was imaged using FLIM (Figure S6 a and b, SI). Consistent with AFM imaging (Fig. 2b, 0 h), GM1 nanodomains are distinguished in both FLIM and FCS studies. The proximal leaflet, which is 100 % DOPC, appears to be homogeneous, but demonstrates a reduced lipid diffusivity of 4.6±0.4 $\mu m^2/s$ (α=0.98) compared to the pristine symmetric DOPC-only bilayer, which has a diffusion coefficient of approximately 5.1±0.4 $\mu m^2/s$ (α=1).[55] Following incubation with 1μM $A\beta_{1\text{-}42}$ (unlabelled), we observed the disintegration of GM1 nanodomains/clusters within 1 hour (Fig. S6d, SI), corroborating our AFM study (vide infra). In addition, distinctly brighter DOPC and GM1 micron scale features (cf. FLIM image highlighted in white rectangular box, Fig. S6c and d, SI) appeared upon prolonged incubation. The emergent features registered each other across both leaflets, although the dimensions of the features were larger in the BODIPY-GM1 channel (upper leaflet) than in the ATTO655-PE channel (lower leaflet) (cf. rectangular white box in Fig.S6c,d (SI)). After 1 hour of peptide incubation, the BODIPY and ATTO probes diffusivity from these aggregated regimes

decreased (Fig. S6g, SI). After 18 hours of peptide incubation, the overall size of the membrane cluster increases (cf. rectangular box in Fig. S6 e and f (SI)) and the corresponding lipid diffusivity decreases further, suggesting that GM1 mediated $A\beta_{1-42}$ aggregates influencing lipid mobility in each leaflet. This is in line with a prior study by Seigneuret et al. that used Laurdan fluorescence to show that $A\beta_{1-42}$ improves the packing of membrane order and increase in domain size in the presence of ganglioside.[56]

3.3 Role of terminal versus branched α2,3-linked sialic acid (SA) residues as receptor for $A\beta_{1-42}$ binding

Gangliosides, sialic-acid (SA) containing glycosphingolipids (GSLs), are predominantly located in the outer leaflet of the plasma membrane and are crucial in the central nervous system, aiding in cell recognition, signal transduction, neuroinflammation, and the structural organization of membrane microdomains. These processes are crucial for preserving the integrity and functionality of the CNS, and any disruption of lipid metabolism, notably concerning GSLs, significantly contributes to the pathogenesis of AD.[57] Postmortem examinations of the brains of Alzheimer's disease patients demonstrated reduced concentrations of branched gangliosides such as GM1, GD1a, GD1b, and GT1b alongside elevated levels of terminal or simple gangliosides GM3 and GM2 in the impacted cortical areas.[58] Structurally, GM1 and GD1a have the same ganglio-tetrose backbone with one and two SA residues, respectively, branched internally off the second backbone sugar and/or in the terminal position, whereas GM3 has a structure similar to GM1's except that it lacks the two terminal sugars of the tetrose backbone, converting its SA from an internal branching residue to a terminal one (Scheme 1). Given the prevalence of various GSLs in AD, we intend to employ our multimodal surface-sensitive approach to elucidate the structural differences in chemical linkages, as well as the positioning of SA receptors and head group charges, which lead to varied binding and aggregation of $A\beta_{1-42}$. Initially, the electrochemical impedance response of different glycosphingolipid containing membranes to exposure to $A\beta_{1-42}$ were compared. Both DOPC:GM1(99:1) and DOPC:GM3 (99:1) asymmetric membranes showed comparable impedance responses (Figs. 2a and 3a,b, black symbol). For membranes comprised of DOPC:GD1a (99:1) and DOPC:GSL (99:1) (where GSL refers to mixed GSLs composed of 98% of GM1, GD1a, GD1b, GT1b gangliosides, with the remaining 2% made up of various gangliosides such as GM2 and GM3) the impedance behaviour was mutually similar but different to that of DOPC:GM1 and DOPC:GM3. The GD1a and GSL containing membranes show a significant reduction in membrane resistance when exposed to $A\beta_{1-42}$, with a slower decline reported in the GSL membrane compared to the GD1a membrane. The response is linear for DOPC:GSL (blue, Fig. 3a) and exponential for DOPC:GD1a (red, Fig. 3a), with the latter attaining electrochemical equilibrium in approximately 12 hours. The overall amplitude of resistance decrease remains significant, with no recovery observed in either case, notably at the intermediate time scale. This suggests that $A\beta_{1-42}$ binds and may cover uniformly through carpet like assemblies at the membrane interface, without forming any aggregates or

assemblies. The corresponding capacitance follows the opposite trend (Fig. 3b), indicative of membrane thinning.

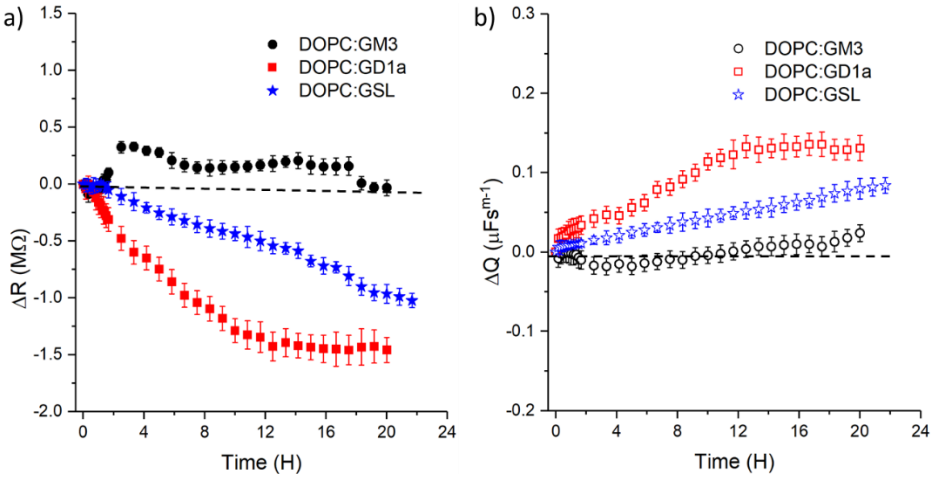


Figure 3. Temporal evolution changes in relative a) resistance (filled symbol) and b) capacitance (open symbols) induced by 1μM $A\beta_{1-42}$ at different asymmetric MSLB membranes such as DOPC:GM3 (black), DOPC:GD1a (red) and DOPC:GSL (blue) with respect to their equilibrated admittance value (shown in horizontal dotted line). All MSLBs were spanned over gold microcavity array electrode using LB-VF method. Error bars represent standard error of the mean (N = 3).

3.3.1 Branched gangliosides receptors inhibited peptide aggregation than terminal GM3. To elucidate the modulation of $A\beta_{1-42}$ binding and aggregate formation by branched and terminal gangliosides receptors at molecular level, AFM experiments were carried out in liquid mode on mica-supported asymmetric lipid bilayers, comprising a lower leaflet DOPC and an outer leaflet containing DOPC with 1 mol% of individual ganglioside receptors, GM3, GD1a or mixture of GSLs. Prior to the administration of $A\beta_{1-42}$, all of the membranes appeared homogeneous (Fig. 4a-c, left panel, 0h), as evident by AFM. Unlike GM1 containing membrane, irregularly shaped sub-microscopic $A\beta_{1-42}$ aggregates are clearly visible at the DOPC:GM3 membrane post 18 hours of incubation (Fig. 4a). The height profile analyses indicate that the peptide aggregates protrude ca. 7-8 nm above the DOPC:GM3. The aggregates thus differ in shape, height and size from the aggregates formed at the DOPC:GM1 membrane. Notably, no such distinct aggregates are observed to form at the DOPC:GD1a membrane, where the image remains uniform, albeit with a modest increase in roughness compared to the peptide free pristine bilayer topography (Fig. 4b), suggesting weaker binding, which is consistent with our subsequent FLIM studies (vide supra). A similar observation i.e., no distinct aggregates are formed at the DOPC:GSL membrane (Fig. 4c). Nonetheless, a scan at the different area after 18 hours revealed carpet-like coverage of $A\beta_{1-42}$ over the DOPC:GSL membrane (right panel, Fig. 4c), corroborating the findings from EIS (Fig. 3) and confocal imaging data (Fig. S7, SI) at MSLBs.

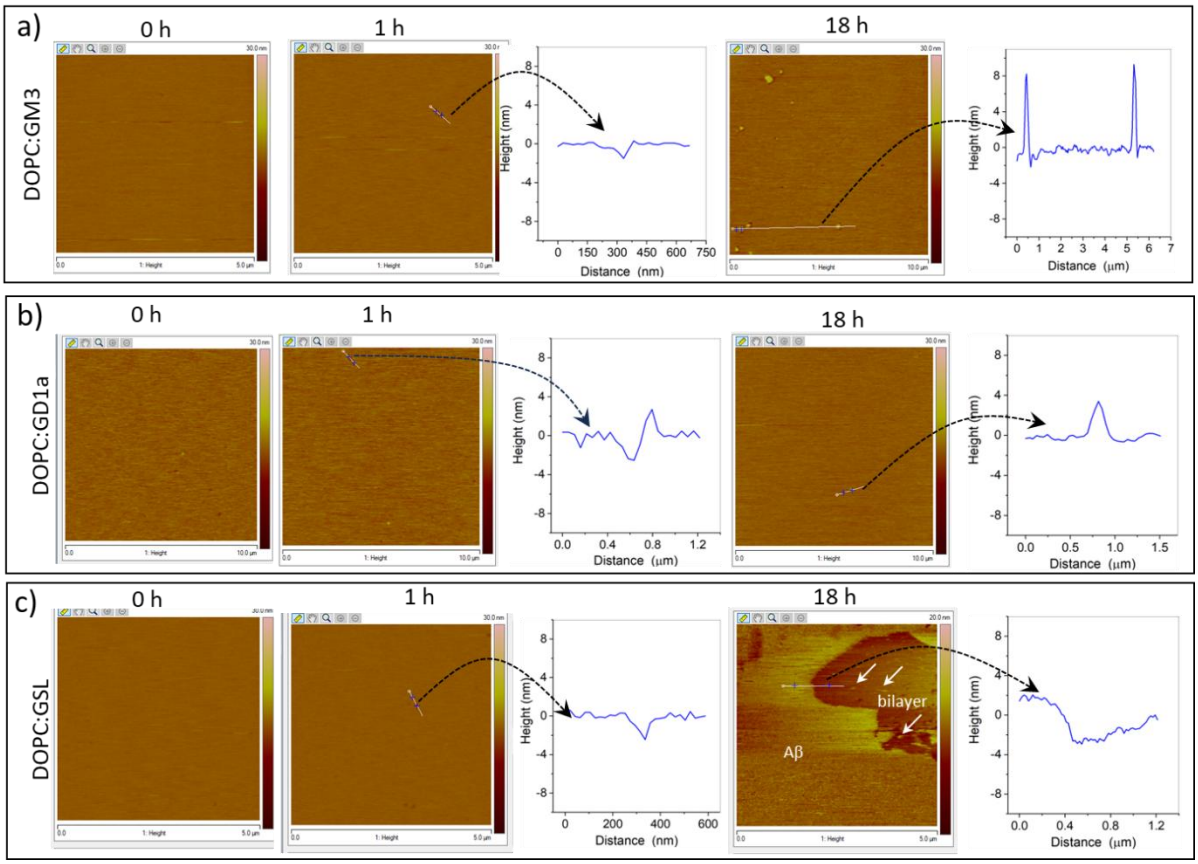


Figure 4. Topographic images of a) DOPC:GM3, b) DOPC:GD1a, and c) DOPC:GSL asymmetric membranes before (0h) and after (1hr and 18h) incubation with 1 μM $A\beta_{1-42}$. The line profile analyses (blue line) corresponding to the spatial regime of topographic images are indicated by black curved arrow.

Subsequent FLIM imaging and lifetime histogram analyses were carried out to clarify the response of distinct GSL receptors to provide binding at the same temporal scale as our AFM studies. The top panels in Figure 5a, d and g show the time-lapse FLIM images obtained from the lipid channel of DOPC:GM3, DOPC:GD1a and DOPC:GSL bilayer before (0h, left), after 1h (centre) and 18 h (right) of $A\beta_{1-42}$ binding, while the bottom panels display the corresponding FLIM images from the Aβ555 channel. The peptide at early time-point, i.e., after 1h (middle panel) did not have significant impact on the membrane homogeneity or on probe lifetime amplitude distribution plots (shown in right panels of Fig. 5a, d, and g). Notably, after 18 hours of incubation with $A\beta_{1-42}$, DOPC:GM3 membrane becomes moderately heterogeneous with the emergence of brightly emissive lipidic nanoclusters (highlighted in red square box) and circular shaped lipid microdomains (white rectangular box). Since peptide aggregates formed at DOPC:GM3 membrane are circular, as indicated by AFM, and below the light diffraction limit, we were only able to observe a limited number of these features in the peptide channel (marked in triangle, bottom right panel Fig. 5a) using FLIM. Again, consistent with EIS and AFM studies for DOPC:GD1a and DOPC:GSL, no aggregates were observed from the peptide channel at this method's resolution even after 18 hours incubation. The FLIM and occurrence amplitude versus lifetime plots from the

peptide channel of DOPC:GD1a and DOPC:GSL membranes showed a moderate association of $A\beta_{1-42}$ to the membrane surface compared to DOPC:GM1 (Fig. 2c) and DOPC:PIP2 (Fig. 1g). This suggests that peptide aggregation is inhibited at DOPC:GD1a and DOPC:GSL membranes but fluorescence imaging indicates that the amyloid monomer does associate with the membrane, without aggregation which is consistent with previous reported data.[59]

FCS from the lipid channel further established the peptide induced DOPC:GM3 membrane heterogeneity. After 1 hour peptide incubation, the overall lipid diffusivity (D = 4.3±0.12 $\mu m^2/s$) remains unchanged when compared to pristine DOPC:GM3 membrane (ACF in black and red, Fig. 5b, acquired from the regime highlighted in circle in panel a). However, the interaction led to the emergence of more fluidic lipid micro domains (highlighted in white rectangular box, panel a, in the lipid channel). The lipid diffusion coefficient associated with these microdomains was measured as 7.1±0.2 $\mu m^2/s$, with an α value of 1 (cf. ACF in blue in Fig. 5b). After 1 h, the mobility of Aβ555 appears to be transiently associated with the DOPC:GM3, as evidenced by a two-component ACF trace (black filled square, Fig. 5b). However, the amplitude of bulk-like peptide mobility with a diffusion coefficient value of 78±8 $\mu m^2/s$ indicates free or weakly associated peptide dominates over the membrane associated fraction of 2D peptide diffusion (indicated by downward arrow, Fig. 5b). After 18 hours, spatially resolved FCS data revealed three distinct but hindered lipid diffusivity populations. The lipid diffusivity values from the homogeneous (white circle), liquid disordered microdomains (white rectangle), and lipid ordered nanocluster (red triangle) regimes were respectively 2±0.08 $\mu m^2/s$ (α = 1) (ACF in open black, Fig. 5c), 3.94±0.10 $\mu m^2/s$ (α = 1) (ACF in open blue, Fig. 5c), and 0.98±0.06 $\mu m^2/s$ (α = 0.87) (ACF in open olive, Fig. 5c). Nonetheless at 18 hours, the Aβ555 diffusion from the membrane surface (highlighted in white circle) remains bulk-like though with the amplitude of this component is reduced as seen in the ACF and associated diffusivity value also reduced to 58±6 $\mu m^2/s$, (cf. ACF in black filled square, Fig. 5c). The amplitude of membrane bound fraction (arrow, Fig. 5c, black) remains weak indicating either monomeric or diffraction limited oligomeric peptide that is weekly associated at the DOPC:GM3 membrane interface. In contrast, the diffusivity of Aβ555 obtained from the aggregates (marked in white triangle) revealed distinct two-component diffusion (obtained by fitting the ACF using equation 3), determined as 0.01±0.01 and 11±2 $\mu m^2/s$ (cf. ACF in red filled square, Fig. 5c) respectively. The $A\beta_{1-42}$ moderately reduced the membrane diffusivity of DOPC:GD1a and DOPC:GSL membrane at early time (1h, ACF in open red, Fig. 5 e,h) but the overall viscosity is much prominent after 18 hours (ACF in open red, Fig. 5f,i). After 1h, the Aβ555 diffusivity value at DOPC:GD1a membrane was determined to be 5.1±0.21 $\mu m^2/s$ (ACF in filled red, Fig. 5e), and this value was further reduced to 2.1 ±0.11 $\mu m^2/s$ after 18h (ACF in filled red, Fig. 5f). These values, which were obtained by fitting the ACF using two-component diffusion fit Eq. (3), are linked to membrane bound fraction and further

imply the absence of peptide aggregation. A relatively greater reduction of peptide diffusion (0.68±0.2 $\mu m^2/s$) was evident after 18 hours of incubation with DOPC:GSL membrane (ACF in filled red, Fig. 5i).

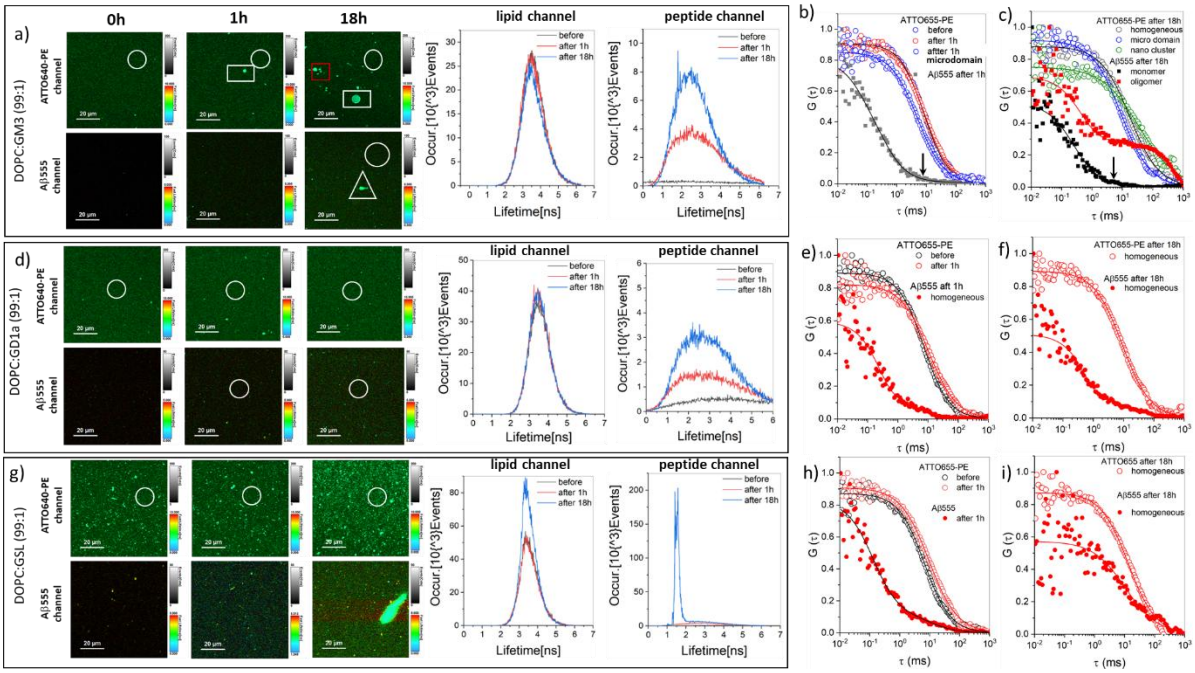


Figure 5. Temporal evolution FLIM images of a) DOPC:GM3, d) DOPC:GD1a, and g) DOPC:GSL asymmetric bilayers supported over glass substrate before (0h) and after 1h and 18h incubation with 1 μM $A\beta_{1-42}$. The top and bottom panels corresponding to panels a, d, and g are the images from lipid (ATTO655-PE) and peptide (Aβ555) channel. The lifetime histogram plots shown in the right top and bottom panel of a, d and g are extracted from the FLIM images at different incubation time intervals (black: 0h; red:1h; blue:18h). b) ACF traces of lipid obtained from the spatially defined homogeneous regime (white circle in Fig. a, 0h) of DOPC:GM3 bilayer membrane before (open black) and after 1h incubation (open red). The ACF shown in open blue (panel b) are from the brighter lipidic micro domain. The Aβ555 ACF trace obtained from the bilayer plane (homogeneous regime) after 1h and 18 h of incubation is shown in filled grey symbol (panel b) and filled black symbol (panel c) respectively. The ACF of peptide after 18 hours obtained from the aggregated region is shown in filled red in panel c. Similarly, in panel e and h, the ACF traces of lipids from DOPC:GD1a and DOPC:GSL before (open black), after 1h (open red) are shown along with the peptide ACF after 1 h incubation is shown in filled red. The respective ACF of lipid (open red) and peptide (filled red) after 18 hours of binding for DOPC:GD1a and DOPC:GSL membrane is shown in panel f and i respectively. All FCS data are fitted using 2D diffusion model equation (1) except the one contains two diffusion time constants are fitted using two-component diffusion model using Eq. (3).

3.4 Disassembly of glycosphingolipid mediated $A\beta_{1-42}$ aggregates by repurposed drugs:

We used AFM to visualize the disassembly of $A\beta_{1-42}$ aggregates generated at different sialic acid receptors, GM1, GM3 and GSL containing DOPC membrane on drug synergism, similar to the approach discussed above for negatively charged PIP2 and DOPS containing membranes. Figure 6a shows the nano dimensioned circular aggregates of $A\beta_{1-42}$ formed at DOPC:GM1 membrane at 18 hour time point. Co-administration of imipramine and fluoxetine successfully eliminates the circular shaped aggregates without damaging the overall integrity of the membrane. This was evident in the decrease in height of these aggregates from 5.5 nm to 1.7 nm within 20 minutes of drug administration. By 90 minutes, most of the surface bound aggregates have been removed though a small number of aggregates appear to be resistant to removal (indicated by white arrow, right panel Fig. 6a).

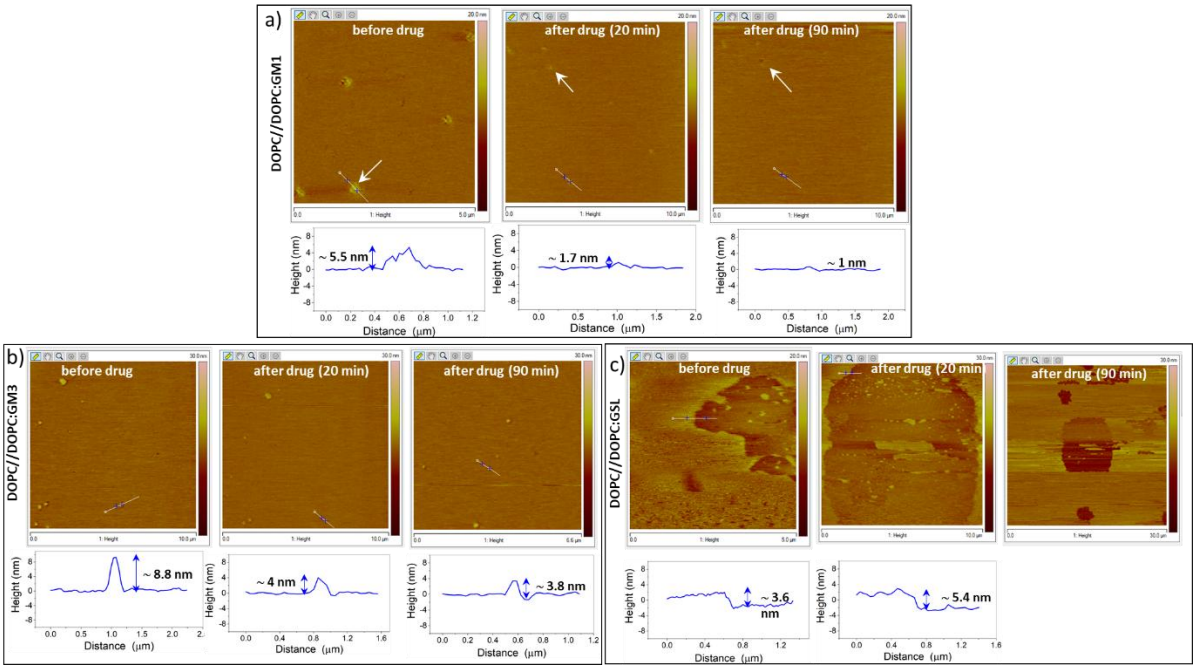


Figure 6. Topographic images showing the impact of drug (10 μM imipramine and 1μM fluoxetine) before and after 20 mins and 90 mins post $A\beta_{1-42}$ associated a) DOPC:GM1, b) DOPC:GM3, and c) DOPC:GSL asymmetric membranes. The line profile analyses corresponding to the region of interest of AFM images are shown in the bottom.

Direct interaction between the drugs and the peptide aggregates is also apparent from the EIS data. When both drugs are administered together to $A\beta_{1-42}$ aggregates at DOPC:GM1, a decrease in membrane admittance is observed (Fig. S8a, SI). In contrast, when the drug is incubated with pristine DOPC:GM1 membrane, it causes an increase in membrane admittance, which attributed to its passive permeation (Fig. S8b, SI), in line with our recent study.[44] Upon preincubation of monomeric $A\beta_{1-42}$ with the drug and subsequent interaction with the DOPC:GM1 membrane resulted in an unchanged resistance up to 4 hours (Fig. S8c, SI), contrasting the trend observed in the absence of drug (Fig. 2a, vide infra).

Thereafter, a gradual decline was noted, indicating that the drug effectively inhibits $A\beta_{1-42}$ aggregate formation at the DOPC:GM1 membrane. The drug combination behaves similarly with $A\beta_{1-42}$ aggregates formed at the DOPC:GM3 membrane (Fig. 6b). By contrast, AFM imaging did not capture any visual distinction before and after drug treatment of the peptide incubated with-DOPC:GD1a membrane (data not shown). While, the carpet-like $A\beta_{1-42}$ assemblies that are formed at DOPC:GSL membrane post 18 hours were removed partially from the bilayer surface within 90 minutes upon drug administration, as evidenced by a wider scan AFM image (Fig. 6c).

4. Discussion

In this study, we compared anionic and glycosphingolipid receptors as anchors and nucleation locations for monomeric $A\beta_{1-42}$ binding and peptide aggregation/assembly formation at DOPC membranes in real-time. This work exploited LB-VF method to create the asymmetric bilayer membrane in the form of MSLB or SLB at various substrates such as gold microcavity imprinted array, glass and mica. Although glycosphingolipids are present in the outer leaflet of the bilayer, typically, neuronal membrane anionic lipid receptors such as PIP2 and DOPS are found on the inner leaflet but are exposed to the outer leaflet in diseased cells[60,61]. Using multimodal interrogation, we observed that the interaction and membrane mediated $A\beta_{1-42}$ aggregate formation is triggered due to electrostatic interaction between the peptide and negatively charged headgroup of PIP2 via pore-formation than that of zwitterionic DOPC membrane. Our EIS analysis, as a very sensitive and label-free technique, reliably predicted the onset time (4-8 hours) of peptide aggregation at negatively charged membranes (Fig. 1a). Typically, the aggregation process at a negatively charged membrane employing EIS is judged by an initial decrease in membrane resistance for 4-8 hours, followed by an increase in resistance as time passed.[26] Static AFM and FLIM images at early (1 h) and prolong (18 h) stage of peptide binding revealed extensive peptide association, aggregation that led to both membrane reorganization and pore formation to the negatively charged membrane (Fig. 1d,g). Lipid diffusivity study using FCS further revealed that the peptide binding increases the overall membrane packing order. Peptide's hindered diffusion is also noted at early stage (1 h) of binding to the negatively charged DOPC:PIP2 membrane. Peptide binding to DOPC:PIP2 induces both gel-like and fluidic lipid microdomains, which appear brighter and have a slower and faster lipid diffusivity respectively, than that of the pristine bilayer diffusion without peptides (Fig. 1h). Currently we do not know why we observe multiple domains form within the $A\beta_{1-42}$ modified membrane; one possibility is the amyloid binding stimulate liquid-liquid phase separation (LLPS) in the membrane. Such behaviour has been noted previously.[62,63] When compared to the carpet-like aggregates generated at negatively charged DOPS containing membrane post 18 hours of peptide binding that we observed previously [26], the aggregates at DOPC:PIP2 membrane remained circular and isolated. These behaviour could be due to a greater affinity of the $A\beta_{1-}$

$_{42}$ peptide to the 2D phase separated PIP2 cluster present in the outer leaflet of the membrane, consistent with a recent study reported by Saleem et al.[64] versus a well-mixed two-component DOPC:DOPS (90:10) bilayer.

Among several glycosphingolipid-containing membranes, we observed that a greater binding and creation of isolated distinct aggregates formed at the DOPC:GM1 (Fig. 2) and DOPC:GM3 (Figs. 3 and 4a) membranes without any pore formation. The aggregation pathways are largely inhibited at DOPC:GD1a and DOPC:GSL membranes within our experimental time window; instead, the binding results indicate weak membrane association. The extent of peptide binding and membrane reorganization, however, remained significantly elevated for GM1 containing membrane. Our result suggests that the presence of increase number of sialic acid (SA) branched group in GD1a or mixed gangliosides, $A\beta_{1-42}$ aggregate formation inhibits but did not restrict receptor binding, which is consistent with previous study.[65]

Considering that negatively charged PIP2, DOPS and glycosphingolipids receptors plays a crucial role in various essential functions in neurons, such as signalling, neuronal and synaptic function, a decrease in receptor levels in presence of Aβ could potentially explain for some symptoms associated in AD,[66] and holds potential interest as a possible target for pharmacological intervention. Our study mimicked the disease cell neuronal model membrane, which contained a lower level of receptors (1 mol%) distributed asymmetrically at the upper leaflet of bilayer. As pharmacological intervention, we then looked at how these membrane/receptor mediated $A\beta_{1-42}$ aggregation can be disassembled from the membrane surface without damaging the integrity of membrane as means of early AD diagnosis using repurposed small molecule drugs. Eliminating surface mediated $A\beta_{1-42}$ aggregates/amyloid plaque prior to their transformation into fibrils could be of interest for early diagnosis because, they are more toxic than $A\beta_{1-42}$ fibrils, and the transition from membrane-mediated oligomers to fibril is a slow process. Our drug synergism approach successfully removed of $A\beta_{1-42}$ aggregates formed at the DOPC:PIP2 (Fig. 1k,l), DOPC:DOPS (Fig. S3a,b), DOPC:GM1 (Fig. 6a) and DOPC:GM3 (Fig. 6b), as confirmed by using AFM and FLIM images within 2 hours. Previously various small molecules have been mixed with peptide oligomers that had resulted weak binding to the membrane. Ginnalin A (GA), a polyphenolic compound isolated from the maple (*Acer rubrum*) and K162[67], a fluorene-based drug, have demonstrated the ability to prevent oligomer formation, and disassemble mature Aβ fibrils into small, nontoxic granular aggregates.[68] Moreever, small synthetic molecules are believed to be modulators of metal ion induced aggregation and disaggregation in a membrane free environment.[69,70] Melacini et al., demonstrated the stronger affinity of catechins based small molecules for Aβ oligomers using NMR spectroscopy.[71] While the aforementioned studies justify the utilization of small molecules as therapeutics for AD, the repurposed drugs (fluoxetine and imipramine) used in this work are cost-effective, CNS+ permeable antidepressants, and our findings

provide direct evidence of the disassembly of receptor-mediated peptide aggregates at high resolution. Although a direct mechanism has not been found, we hypothesize that the aromatic rings of the drugs interact more favorably with the aromatic/hydrophobic amino acid side chains (LVFFA, cf. Scheme 1j) located in the core region of $A\beta_{1-42}$, which is crucial for Aβ aggregation[72–75], leading to the disassembly of aggregates.

Furthermore, it is believed that the oligomeric structure of Aβ peptide is more toxic than its fibrillogenic form, which is typically generated via maturation of membrane mediated oligomers or upon self-aggregation of Aβ at high concentrations in a membrane free environment. The kinetic mechanism that drive amyloid fibril production from its monomeric counterpart is complex and involves multiple steps.[76] As previously noted, we did not notice fibril-like $A\beta_{1-42}$ from its monomeric counterparts in our experimental setting. We are intrigued to examine how these combined drugs respond to the fibrils. To test this hypothesis, we first prepared oligomers/protofibrils in HEPES buffer by ageing $A\beta_{1-42}$ in a membrane free environment at relatively excess concentration of 0.1 mM for more than 3 weeks at 4°C. The preformed oligomers are diluted to a working concentration of 0.25 μM and subsequently added to the zwitterionic DOPC SLB. At this stage, no specific receptors are included in the membrane to see whether the fibril growth is independent of any specific receptor. Our FLIM study reveals that fibrillation process is not halted in pristine DOPC membrane (Fig. S9, SI). During the fibrillation process, membrane reorganization occurs, which may result in the development of pores. After 18 hours of fibrillar growth, we incubate with drug, and found no disassembly of fibrils, suggesting that the choice of drug synergism explored in this study had no effect on membrane mediated fibrils, at least within 24 h experimental window. Given the lack of appropriate medication, our in vitro studies in a cell free environment provided some promising discoveries. The choice drug synergism has the potential, at least in part, to disassemble the membrane mediated aggregates before transitioning into fibrils, as in the case for early stages of AD, and can thus be revisited for cell-based assays in AD research.

5. Conclusions

In summary, multimodal analysis; EIS, AFM, FLIM and FCS applied to pore and planar supported lipid membranes shows that the presence, dynamics and structure of monomeric $A\beta_{1-42}$ membrane-mediated assembly and disassembly are strongly influenced by the identity of the membrane receptor. Real-time membrane admittance data from EIS showed evidence of pore-formation, membrane insertion, variation of membrane thickness , and the onset time for $A\beta_{1-42}$ aggregation formation. AFM imaging corroborated the EIS findings, demonstrating that membrane pore-formation occurred following $A\beta_{1-42}$ binding to negatively charged DOPC:PIP2 membrane, but binding to glycosphingolipid-containing receptors was surface associated without any pore-formation. Among different glycosphingolipids,

circular aggregates develop at GM1 and GM3 containing membranes, whereas at GD1a and mixed GSLs containing DOPC membrane, such aggregates were absent. Fluorescence lifetime imaging and spatially resolved FCS indicate the emergence of liquid-disordered and ordered domains, associated by fast and slow lipid diffusion upon amyloid peptide binding. The overall lipid and peptide's diffusivity is decreased but the extent to which this decrease is depended on the physicochemical properties of receptors.

Additionally, we demonstrate that two antidepressants imipramine and fluoxetine work synergistically to disassemble $A\beta_{1-42}$ aggregates formed at membranes containing GM1, GM3, or negatively charged lipids such as DOPS and PIP2 within a couple of hours. Since fibril formation proceeds from oligomers/aggregate, disassembling the latter entities may prevent fibril formation. Together, these results provide mechanistic insights into the biophysics of $A\beta_{1-42}$ binding, assembly and disassembly and may be helpful to suggest constraints on host cell tropism and possible AD treatment therapy.

Supporting Information

This article contains supporting information. Details of additional FLIM, EIS, AFM and confocal images were provided.

Author contributions

Nirod Kumar Sarangi: Conceptualization, Methodology, Investigation, Formal analysis, Writing – original draft, Writing – review & editing; **Subrata Mondal**: Investigation, Formal analysis, Writing-review & editing; **Tia E. Keyes**: Conceptualization, Resources, Funding acquisition, Supervision, Writing – review & editing, Project supervision.

Declaration of Competing Interest

The authors declare that they have no known competing financial interests or personal relationships that could have appeared to influence the work reported in this paper.

Acknowledgements

This material is based upon work supported by Science Foundation Ireland under Grant No. [14/IA/2488], [19/FFP/6428], [12/RC/2276_P2] and [14/IA/2488], [19/FFP/6428] and [12/RC/2276_P2].

References:

[1] H. Hampel, J. Hardy, K. Blennow, C. Chen, G. Perry, S.H. Kim, V.L. Villemagne, P. Aisen, M. Vendruscolo, T. Iwatsubo, C.L. Masters, M. Cho, L. Lannfelt, J.L. Cummings, A. Vergallo, The Amyloid-β Pathway in Alzheimer's Disease, Mol. Psychiatry. 26 (2021) 5481–5503. doi:10.1038/s41380-021-01249-0.

[2] S. Schiavone, P. Tucci, E. Mhillaj, M. Bove, L. Trabace, M.G. Morgese, Antidepressant drugs for beta amyloid-induced depression: A new standpoint?, Prog. Neuro-Psychopharmacology Biol. Psychiatry. 78 (2017) 114–122. doi:10.1016/j.pnpbp.2017.05.004.

[3] F. Caraci, F. Tascedda, S. Merlo, C. Benatti, S.F. Spampinato, A. Munafò, G.M. Leggio, F. Nicoletti, N. Brunello, F. Drago, M.A. Sortino, A. Copani, Fluoxetine Prevents Aβ1-42-Induced Toxicity via a Paracrine Signaling Mediated by Transforming-Growth-Factor-β1, Front. Pharmacol. 7 (2016). doi:10.3389/fphar.2016.00389.

[4] R. Khoury, G.T. Grossberg, Impact of Antidepressant Use on the Trajectory of Alzheimer's Disease: Evidence, Mechanisms, and Therapeutic Implications, CNS Drugs. 33 (2019) 17–29. doi:10.1007/s40263-018-0590-9.

[5] M. Lozupone, M. La Montagna, F. D'Urso, C. Piccininni, A. Rinaldi, M. Beghi, C.M. Cornaggia, R. Sardone, V. Solfrizzi, A. Daniele, D. Seripa, G. Giannelli, A. Bellomo, F. Panza, The Challenge of Antidepressant Therapeutics in Alzheimer's Disease, in: 2020: pp. 267–281. doi:10.1007/978-3-030-42667-5_10.

[6] M. Buttini, G.-Q. Yu, K. Shockley, Y. Huang, B. Jones, E. Masliah, M. Mallory, T. Yeo, F.M. Longo, L. Mucke, Modulation of Alzheimer-Like Synaptic and Cholinergic Deficits in Transgenic Mice by Human Apolipoprotein E Depends on Isoform , Aging, and Overexpression of Amyloid β Peptides But Not on Plaque Formation, J. Neurosci. 22 (2002) 10539–10548. doi:10.1523/JNEUROSCI.22-24-10539.2002.

[7] A.S. Correia, N. Vale, Antidepressants in Alzheimer's Disease: A Focus on the Role of Mirtazapine, Pharmaceuticals. 14 (2021) 930. doi:10.3390/ph14090930.

[8] G. Tin, T. Mohamed, A. Shakeri, A.T. Pham, P.P.N. Rao, Interactions of Selective Serotonin Reuptake Inhibitors with β-Amyloid, ACS Chem. Neurosci. 10 (2019) 226–234. doi:10.1021/acschemneuro.8b00160.

[9] R. Keowkase, M. Aboukhatwa, Y. Luo, Fluoxetine protects against amyloid-beta toxicity, in part via daf-16 mediated cell signaling pathway, in Caenorhabditis elegans, Neuropharmacology. 59 (2010) 358–365. doi:10.1016/j.neuropharm.2010.04.008.

[10] T. Guo, D. Zhang, Y. Zeng, T.Y. Huang, H. Xu, Y. Zhao, Molecular and cellular mechanisms underlying the pathogenesis of Alzheimer's disease, Mol. Neurodegener. 15 (2020) 40. doi:10.1186/s13024-020-00391-7.

[11] D.A. Butterfield, A.M. Swomley, R. Sultana, Amyloid β -Peptide (1–42)-Induced Oxidative Stress in Alzheimer Disease: Importance in Disease Pathogenesis and Progression, Antioxid. Redox Signal. 19 (2013) 823–835. doi:10.1089/ars.2012.5027.

[12] U. Sengupta, A.N. Nilson, R. Kayed, The Role of Amyloid-β Oligomers in Toxicity, Propagation, and Immunotherapy, EBioMedicine. 6 (2016) 42–49. doi:10.1016/j.ebiom.2016.03.035.

[13] T. Wisniewski, J. Ghiso, B. Frangione, Peptides homologous to the amyloid protein of Alzheimer's disease containing a glutamine for glutamic acid substitution have accelerated amyloid fibril formation, Biochem. Biophys. Res. Commun. 179 (1991) 1247–1254. doi:10.1016/0006-291X(91)91706-I.

[14] S. Sonnino, A. Prinetti, L. Mauri, V. Chigorno, G. Tettamanti, Dynamic and Structural Properties of Sphingolipids as Driving Forces for the Formation of Membrane Domains, Chem. Rev. 106 (2006) 2111–2125. doi:10.1021/cr0100446.

[15] K. Simons, W.L.C. Vaz, Model Systems, Lipid Rafts, and Cell Membranes, Annu. Rev. Biophys. Biomol. Struct. 33 (2004) 269–295. doi:10.1146/annurev.biophys.32.110601.141803.

[16] D. Mrdenovic, M. Majewska, I.S. Pieta, P. Bernatowicz, R. Nowakowski, W. Kutner, J. Lipkowski, P. Pieta, Size-Dependent Interaction of Amyloid β Oligomers with Brain Total Lipid Extract Bilayer—Fibrillation Versus Membrane Destruction, Langmuir. 35 (2019) 11940–11949. doi:10.1021/acs.langmuir.9b01645.

[17] K. Yanagisawa, Pathological significance of ganglioside clusters in Alzheimer's disease, J. Neurochem. 116 (2011) 806–812. doi:10.1111/j.1471-4159.2010.07006.x.

[18] M. Sakono, T. Zako, Amyloid oligomers: formation and toxicity of Aβ oligomers, FEBS J. 277 (2010) 1348–1358. doi:10.1111/j.1742-4658.2010.07568.x.

[19] K. Yanagisawa, A. Odaka, N. Suzuki, Y. Ihara, GM1 ganglioside–bound amyloid β–protein (Aβ): A possible form of preamyloid in Alzheimer's disease, Nat. Med. 1 (1995) 1062–1066. doi:10.1038/nm1095-1062.

[20] K. Yanagisawa, Role of gangliosides in Alzheimer's disease, Biochim. Biophys. Acta - Biomembr. 1768 (2007) 1943–1951. doi:10.1016/j.bbamem.2007.01.018.

[21] K. Yanagisawa, GM1 ganglioside and Alzheimer's disease, Glycoconj. J. 32 (2015) 87–91. doi:10.1007/s10719-015-9579-5.

[22] T. Matsubara, K. Iijima, N. Yamamoto, K. Yanagisawa, T. Sato, Density of GM1 in Nanoclusters Is a Critical Factor in the Formation of a Spherical Assembly of Amyloid β-Protein on Synaptic Plasma Membranes, Langmuir. 29 (2013) 2258–2264. doi:10.1021/la3038999.

[23] T. Matsubara, M. Nishihara, H. Yasumori, M. Nakai, K. Yanagisawa, T. Sato, Size and Shape of Amyloid Fibrils Induced by Ganglioside Nanoclusters: Role of Sialyl Oligosaccharide in Fibril Formation, Langmuir. 33 (2017) 13874–13881. doi:10.1021/acs.langmuir.7b02091.

[24] N. Yamamoto, E. Matsubara, S. Maeda, H. Minagawa, A. Takashima, W. Maruyama, M. Michikawa, K. Yanagisawa, A Ganglioside-induced Toxic Soluble Aβ Assembly, J. Biol. Chem. 282 (2007) 2646–2655. doi:10.1074/jbc.M606202200.

[25] E. Evangelisti, R. Cascella, M. Becatti, G. Marrazza, C.M. Dobson, F. Chiti, M. Stefani, C. Cecchi, Binding affinity of amyloid oligomers to cellular membranes is a generic indicator of cellular dysfunction in protein misfolding diseases, Sci. Rep. 6 (2016) 32721. doi:10.1038/srep32721.

[26] J. Robinson, N.K. Sarangi, T.E. Keyes, Role of phosphatidylserine in amyloid-beta oligomerization at asymmetric phospholipid bilayers, Phys. Chem. Chem. Phys. 25 (2023) 7648–7661. doi:10.1039/D2CP03344E.

[27] E. Abramov, I. Dolev, H. Fogel, G.D. Ciccotosto, E. Ruff, I. Slutsky, Amyloid-β as a positive endogenous regulator of release probability at hippocampal synapses, Nat. Neurosci. 12 (2009) 1567–1576. doi:10.1038/nn.2433.

[28] S. Banerjee, M. Hashemi, K. Zagorski, Y.L. Lyubchenko, Cholesterol in Membranes Facilitates Aggregation of Amyloid β Protein at Physiologically Relevant Concentrations, ACS Chem. Neurosci. 12 (2021) 506–516. doi:10.1021/acschemneuro.0c00688.

[29] J.M. Kenyaga, Q. Cheng, W. Qiang, Early stage β-amyloid-membrane interactions modulate lipid dynamics and influence structural interfaces and fibrillation, J. Biol. Chem. 298 (2022) 102491. doi:10.1016/j.jbc.2022.102491.

[30] A. Laganowsky, E. Reading, T.M. Allison, M.B. Ulmschneider, M.T. Degiacomi, A.J. Baldwin, C. V. Robinson, Membrane proteins bind lipids selectively to modulate their structure and function, Nature. 510 (2014) 172–175. doi:10.1038/nature13419.

[31] R. Phillips, T. Ursell, P. Wiggins, P. Sens, Emerging roles for lipids in shaping membrane-protein function, Nature. 459 (2009) 379–385. doi:10.1038/nature08147.

[32] G. Melillo, How Biogen's Aduhelm Approval Marks a Precipitous Turning Point for the FDA, Am. J.

Manag. Care. (2021) July 14. https://www.ajmc.com/view/how-biogen-s-aduhelm-approval-marks-a-precipitous-turning-point-for-the-fda.

[33] T.-W. Kim, Drug Repositioning Approaches for the Discovery of New Therapeutics for Alzheimer's Disease, Neurotherapeutics. 12 (2015) 132–142. doi:10.1007/s13311-014-0325-7.

[34] N.R. Johnson, A.C.-J. Wang, C. Coughlan, S. Sillau, E. Lucero, L. Viltz, N. Markham, C. Allen, A.R. Dhanasekaran, H.J. Chial, H. Potter, Imipramine and olanzapine block apoE4-catalyzed polymerization of Aβ and show evidence of improving Alzheimer's disease cognition, Alzheimers. Res. Ther. 14 (2022) 88. doi:10.1186/s13195-022-01020-9.

[35] J. Bieschke, J. Russ, R.P. Friedrich, D.E. Ehrnhoefer, H. Wobst, K. Neugebauer, E.E. Wanker, EGCG remodels mature α-synuclein and amyloid-β fibrils and reduces cellular toxicity, Proc. Natl. Acad. Sci. 107 (2010) 7710–7715. doi:10.1073/pnas.0910723107.

[36] C.A. Sallaberry, B.J. Voss, W.B. Stone, F. Estrada, A. Bhatia, J.D. Soto, C.W. Griffin, C.M. Vander Zanden, Curcumin Reduces Amyloid Beta Oligomer Interactions with Anionic Membranes, ACS Chem. Neurosci. 14 (2023) 4026–4038. doi:10.1021/acschemneuro.3c00512.

[37] F. Yang, G.P. Lim, A.N. Begum, O.J. Ubeda, M.R. Simmons, S.S. Ambegaokar, P.P. Chen, R. Kayed, C.G. Glabe, S.A. Frautschy, G.M. Cole, Curcumin Inhibits Formation of Amyloid β Oligomers and Fibrils, Binds Plaques, and Reduces Amyloid in Vivo, J. Biol. Chem. 280 (2005) 5892–5901. doi:10.1074/jbc.M404751200.

[38] I. Doytchinova, M. Atanasova, E. Salamanova, S. Ivanov, I. Dimitrov, Curcumin Inhibits the Primary Nucleation of Amyloid-Beta Peptide: A Molecular Dynamics Study, Biomolecules. 10 (2020) 1323. doi:10.3390/biom10091323.

[39] N.K. Sarangi, M. Shafaq-Zadah, G.B. Berselli, J. Robinson, E. Dransart, A. Di Cicco, D. Lévy, L. Johannes, T.E. Keyes, Galectin-3 Binding to α 5 β 1 Integrin in Pore Suspended Biomembranes, J. Phys. Chem. B. 126 (2022) 10000–10017. doi:10.1021/acs.jpcb.2c05717.

[40] S. Ramadurai, N.K. Sarangi, S. Maher, N. Macconnell, A.M. Bond, D. McDaid, D. Flynn, T.E. Keyes, Microcavity-Supported Lipid Bilayers; Evaluation of Drug-Lipid Membrane Interactions by Electrochemical Impedance and Fluorescence Correlation Spectroscopy, Langmuir. 35 (2019). doi:10.1021/acs.langmuir.9b01028.

[41] P.C. Gufler, D. Pum, U.B. Sleytr, B. Schuster, Highly robust lipid membranes on crystalline S-layer supports investigated by electrochemical impedance spectroscopy, Biochim. Biophys. Acta - Biomembr. 1661 (2004) 154–165. doi:10.1016/j.bbamem.2003.12.009.

[42] P. Kapusta, R. Macháň, A. Benda, M. Hof, Fluorescence Lifetime Correlation Spectroscopy (FLCS): Concepts, Applications and Outlook, Int. J. Mol. Sci. 13 (2012) 12890–12910. doi:10.3390/ijms131012890.

[43] C.-C. Weber, G.P. Eckert, W.E. Müller, Effects of Antidepressants on the Brain/Plasma Distribution of Corticosterone, Neuropsychopharmacology. 31 (2006) 2443–2448. doi:10.1038/sj.npp.1301076.

[44] N.K. Sarangi, A. Prabhakaran, M. Roantree, T.E. Keyes, Evaluation of the passive permeability of antidepressants through pore-suspended lipid bilayer, Colloids Surfaces B Biointerfaces. 234 (2024) 113688. doi:10.1016/j.colsurfb.2023.113688.

[45] R. Cukalevski, B. Boland, B. Frohm, E. Thulin, D. Walsh, S. Linse, Role of Aromatic Side Chains in Amyloid β-Protein Aggregation, ACS Chem. Neurosci. 3 (2012) 1008–1016. doi:10.1021/cn300073s.

[46] S. Sipione, J. Monyror, D. Galleguillos, N. Steinberg, V. Kadam, Gangliosides in the Brain: Physiology, Pathophysiology and Therapeutic Applications, Front. Neurosci. 14 (2020). doi:10.3389/fnins.2020.572965.

[47] A. Prinetti, N. Loberto, V. Chigorno, S. Sonnino, Glycosphingolipid behaviour in complex membranes, Biochim. Biophys. Acta - Biomembr. 1788 (2009) 184–193. doi:10.1016/j.bbamem.2008.09.001.

[48] L.B. Sagle, L.K. Ruvuna, J.M. Bingham, C. Liu, P.S. Cremer, R.P. Van Duyne, Single Plasmonic Nanoparticle Tracking Studies of Solid Supported Bilayers with Ganglioside Lipids, J. Am. Chem. Soc.

134 (2012) 15832–15839. doi:10.1021/ja3054095.

[49] R. Šachl, M. Amaro, G. Aydogan, A. Koukalová, I.I. Mikhalyov, I.A. Boldyrev, J. Humpolíčková, M. Hof, On multivalent receptor activity of GM1 in cholesterol containing membranes, Biochim. Biophys. Acta - Mol. Cell Res. 1853 (2015) 850–857. doi:10.1016/j.bbamcr.2014.07.016.

[50] J. Shi, T. Yang, S. Kataoka, Y. Zhang, A.J. Diaz, P.S. Cremer, GM 1 Clustering Inhibits Cholera Toxin Binding in Supported Phospholipid Membranes, J. Am. Chem. Soc. 129 (2007) 5954–5961. doi:10.1021/ja069375w.

[51] C. Yuan, L.J. Johnston, Atomic Force Microscopy Studies of Ganglioside GM1 Domains in Phosphatidylcholine and Phosphatidylcholine/Cholesterol Bilayers, Biophys. J. 81 (2001) 1059–1069. doi:10.1016/S0006-3495(01)75763-3.

[52] L.R. Jordan, M.E. Blauch, A.M. Baxter, J.L. Cawley, N.J. Wittenberg, Influence of brain gangliosides on the formation and properties of supported lipid bilayers, Colloids Surfaces B Biointerfaces. 183 (2019) 110442. doi:10.1016/j.colsurfb.2019.110442.

[53] N.K. Sarangi, P.I. Ilanila, K.G. Ayappa, S.S. Visweswariah, J.K. Basu, Super-resolution Stimulated Emission Depletion-Fluorescence Correlation Spectroscopy Reveals Nanoscale Membrane Reorganization Induced by Pore-Forming Proteins, Langmuir. 32 (2016). doi:10.1021/acs.langmuir.6b01848.

[54] A. Roy, N.K. Sarangi, S. Ghosh, A. Prabhakaran, T.E. Keyes, Leaflet by Leaflet Synergistic Effects of Antimicrobial Peptides on Bacterial and Mammalian Membrane Models, J. Phys. Chem. Lett. 14 (2023) 3920–3928. doi:10.1021/acs.jpclett.3c00119.

[55] L. Zhang, S. Granick, Lipid diffusion compared in outer and inner leaflets of planar supported bilayers, J. Chem. Phys. 123 (2005) 211104. doi:10.1063/1.2138699.

[56] G. Staneva, N. Puff, S. Stanimirov, T. Tochev, M.I. Angelova, M. Seigneuret, The Alzheimer's disease amyloid-β peptide affects the size-dynamics of raft-mimicking Lo domains in GM1-containing lipid bilayers, Soft Matter. 14 (2018) 9609–9618. doi:10.1039/C8SM01636D.

[57] O.K. Inci, H. Basırlı, M. Can, S. Yanbul, V. Seyrantepe, Gangliosides as Therapeutic Targets for Neurodegenerative Diseases, J. Lipids. 2024 (2024) 1–10. doi:10.1155/2024/4530255.

[58] A.J. Hülsmeier, Glycosphingolipids in neurodegeneration – Molecular mechanisms, cellular roles, and therapeutic perspectives, Neurobiol. Dis. 207 (2025) 106851. doi:10.1016/j.nbd.2025.106851.

[59] T. Matsubara, T. Kojima, R. Fukuda, K. Iijma, M. Hirai, N. Yamamoto, K. Yanagisawa, T. Sato, Responsibility of lipid compositions for the amyloid ß assembly induced by ganglioside nanoclusters in mouse synaptosomal membranes, Polym. J. 50 (2018) 745–752. doi:10.1038/s41428-018-0041-y.

[60] R.O. Calderón, G.H. DeVries, Lipid composition and phospholipid asymmetry of membranes from a Schwann cell line., J. Neurosci. Res. 49 (1997) 372–80. http://www.ncbi.nlm.nih.gov/pubmed/9260748.

[61] M. Tsuchiya, Y. Hara, M. Okuda, K. Itoh, R. Nishioka, A. Shiomi, K. Nagao, M. Mori, Y. Mori, J. Ikenouchi, R. Suzuki, M. Tanaka, T. Ohwada, J. Aoki, M. Kanagawa, T. Toda, Y. Nagata, R. Matsuda, Y. Takayama, M. Tominaga, M. Umeda, Cell surface flip-flop of phosphatidylserine is critical for PIEZO1-mediated myotube formation, Nat. Commun. 9 (2018) 2049. doi:10.1038/s41467-018-04436-w.

[62] S. Meker, H. Chin, T.N. Sut, N.-J. Cho, Amyloid-β Peptide Triggers Membrane Remodeling in Supported Lipid Bilayers Depending on Their Hydrophobic Thickness, Langmuir. 34 (2018) 9548–9560. doi:10.1021/acs.langmuir.8b01196.

[63] R. Kobayashi, H. Nabika, Liquid–liquid phase separation induced by crowding condition affects amyloid-β aggregation mechanism, Soft Matter. 20 (2024) 5331–5342. doi:10.1039/D4SM00470A.

[64] A. Tiwari, S. Pradhan, A. Sannigrahi, A.K. Mahakud, S. Jha, K. Chattopadhyay, M. Biswas, M. Saleem, Interplay of lipid head group and packing defects in driving amyloid-beta–mediated myelin-like model membrane deformation, J. Biol. Chem. 299 (2023) 104653. doi:10.1016/j.jbc.2023.104653.

[65] A. Kakio, S. Nishimoto, K. Yanagisawa, Y. Kozutsumi, K. Matsuzaki, Interactions of Amyloid β-Protein with Various Gangliosides in Raft-Like Membranes: Importance of GM1 Ganglioside-Bound Form as an Endogenous Seed for Alzheimer Amyloid, Biochemistry. 41 (2002) 7385–7390. doi:10.1021/bi0255874.

[66] D.E. Berman, C. Dall'Armi, S. V Voronov, L.B.J. McIntire, H. Zhang, A.Z. Moore, A. Staniszewski, O. Arancio, T.-W. Kim, G. Di Paolo, Oligomeric amyloid-β peptide disrupts phosphatidylinositol-4,5-bisphosphate metabolism, Nat. Neurosci. 11 (2008) 547–554. doi:10.1038/nn.2100.

[67] Q. Fan, Y. Liu, X. Wang, Z. Zhang, Y. Fu, L. Liu, P. Wang, H. Ma, H. Ma, N.P. Seeram, J. Zheng, F. Zhou, Ginnalin A Inhibits Aggregation, Reverses Fibrillogenesis, and Alleviates Cytotoxicity of Amyloid β(1–42), ACS Chem. Neurosci. 11 (2020) 638–647. doi:10.1021/acschemneuro.9b00673.

[68] D. Mrdenovic, P. Zarzycki, M. Majewska, I.S. Pieta, R. Nowakowski, W. Kutner, J. Lipkowski, P. Pieta, Inhibition of Amyloid β-Induced Lipid Membrane Permeation and Amyloid β Aggregation by K162, ACS Chem. Neurosci. 12 (2021) 531–541. doi:10.1021/acschemneuro.0c00754.

[69] S.S. Hindo, A.M. Mancino, J.J. Braymer, Y. Liu, S. Vivekanandan, A. Ramamoorthy, M.H. Lim, Small Molecule Modulators of Copper-Induced Aβ Aggregation, J. Am. Chem. Soc. 131 (2009) 16663–16665. doi:10.1021/ja907045h.

[70] J.-S. Choi, J.J. Braymer, R.P.R. Nanga, A. Ramamoorthy, M.H. Lim, Design of small molecules that target metal-Aβ species and regulate metal-induced Aβ aggregation and neurotoxicity, Proc. Natl. Acad. Sci. 107 (2010) 21990–21995. doi:10.1073/pnas.1006091107.

[71] R. Ahmed, J. Huang, R. Lifshitz, K. Martinez Pomier, G. Melacini, Structural determinants of the interactions of catechins with Aβ oligomers and lipid membranes, J. Biol. Chem. 298 (2022) 101502. doi:10.1016/j.jbc.2021.101502.

[72] G. Chen, T. Xu, Y. Yan, Y. Zhou, Y. Jiang, K. Melcher, H.E. Xu, Amyloid beta: structure, biology and structure-based therapeutic development, Acta Pharmacol. Sin. 38 (2017) 1205–1235. doi:10.1038/aps.2017.28.

[73] S.A. Kotler, P. Walsh, J.R. Brender, A. Ramamoorthy, Differences between amyloid-β aggregation in solution and on the membrane: insights into elucidation of the mechanistic details of Alzheimer's disease, Chem. Soc. Rev. 43 (2014) 6692–6700. doi:10.1039/C3CS60431D.

[74] M. Bokvist, F. Lindström, A. Watts, G. Gröbner, Two Types of Alzheimer's β-Amyloid (1–40) Peptide Membrane Interactions: Aggregation Preventing Transmembrane Anchoring Versus Accelerated Surface Fibril Formation, J. Mol. Biol. 335 (2004) 1039–1049. doi:10.1016/j.jmb.2003.11.046.

[75] N.S. de Groot, F.X. Aviles, J. Vendrell, S. Ventura, Mutagenesis of the central hydrophobic cluster in Aβ42 Alzheimer's peptide, FEBS J. 273 (2006) 658–668. doi:10.1111/j.1742-4658.2005.05102.x.

[76] I. Sedov, D. Khaibrakhmanova, Molecular Mechanisms of Inhibition of Protein Amyloid Fibril Formation: Evidence and Perspectives Based on Kinetic Models, Int. J. Mol. Sci. 23 (2022) 13428. doi:10.3390/ijms232113428.